Relativistic heavy ion collisions and string theory

Steve Gubser (Princeton University)
in collaboration with Josh Friess, Georgios Michalogiorgakis,
and Silviu Pufu

Prospects in Theoretical Physics 2006

draft date: July 28, 2006

Contents

1. Introduction

The Relativistic Heavy Ion Collider (RHIC), operating at Brookhaven National Laboratory (BNL), collides gold on gold.

1. Total center of mass energy is about $39\,\mathrm{TeV}$.
2. Roughly 5000 charged particles emerge.
3. There is good evidence that a thermalized quark-gluon plasma (QGP) forms with temperature above the confinement scale.

The theoretical understanding of RHIC physics is imperfect.

1. The QGP is strongly coupled, so perturbative QCD is of limited utility.
2. Lattice calculations provide good information about static properties (like $T_c \approx 170\,\mathrm{MeV}$ for confinement) but not transport properties (like viscosity).
3. String theory, in particular AdS/CFT, offers an alternative description of strongly coupled gauge theory.

Two main themes of the AdS/CFT - RHIC connection are

A The viscosity bound $\eta/s \geq \hbar/4\pi$.

B Jet-quenching and the drag force on hard partons, especially heavy quarks.

A has been under discussion for about 5 years. B is a relatively new development.

2. RHIC primer

We have borrowed freely from the recent review [1], which is a readable account of experimental results to date and their interpretation. An authoritative account of results through 2005 is contained in [2, 3, 4, 5].

2.1. The experimental setup

RHIC accelerates beams of gold nuclei in opposite directions and collides them. Some parameters of the machine:

- The main ring is $3.8\,\mathrm{km}$ in circumference.
- Four experiments (BRAHMS, PHENIX, PHOBOS, and STAR) with complementary capabilities are cited at four of the six beam intersection points.
- The beam energy is $100\,\mathrm{GeV}$ per nucleon, and RHIC can handle other species, e.g. copper. So the number to remember is $\sqrt{s_{NN}} = 200\,\mathrm{GeV}$: that's cm energy per nucleon per nucleon.
- Gold nuclei have 79 protons and 118 neutrons. They are fairly spherical, with a radius R of about $7\,\mathrm{fm}$.
- Lorentz contraction with $\gamma \approx 100$ gives a front-to-back length of $2R/\gamma \approx 0.14\,\mathrm{fm}$.

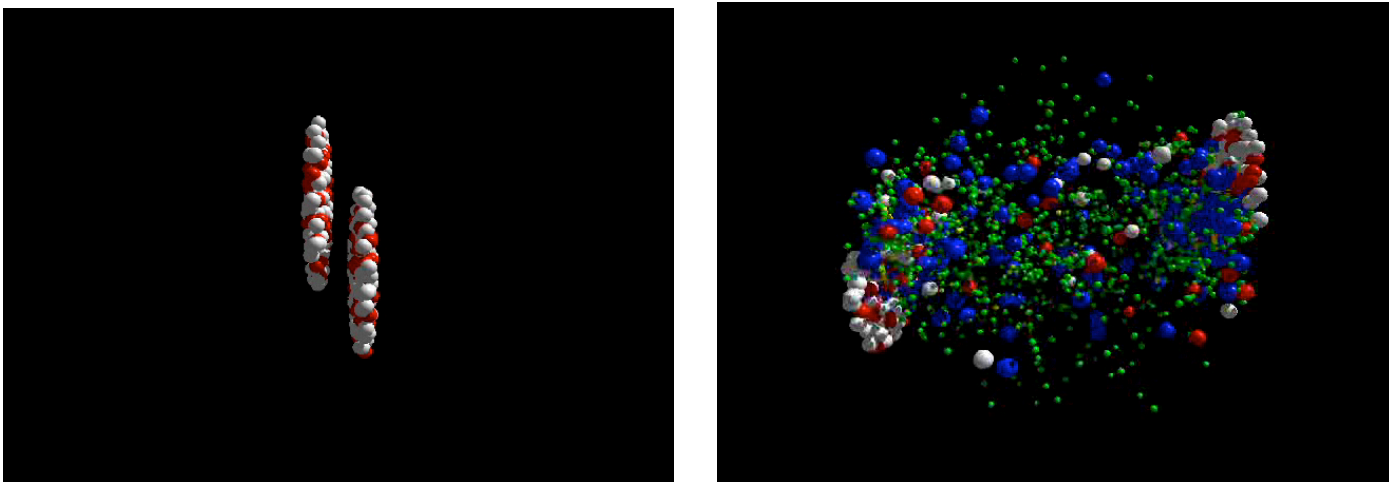

Figure 1: *Ultra-relativistic quantum molecular dynamics simulation of a gold-gold collision [6], with view before (left) and after (right). Species are probably: protons (red), neutrons (white), meson (green), and excited baryons (blue).*

- The inelastic gold-on-gold cross-section may be estimated *roughly* as $\sigma_{\rm tot} = 4\pi R^2$: this is just geometric overlap.

  Exercise 1 (Total cross inelastic cross section) *Compute $\sigma_{\rm tot}$ in barns. About how many gold-gold collisions has RHIC produced?*

  Answer □

- RHIC's design luminosity is $2 \times 10^{26}\,{\rm cm}^{-2}{\rm s}^{-1}$. Integrated luminosity to date is in the ballpark of $4\,{\rm nb}^{-1}$.

- An idealized version of RHIC detectors is the ability to assign p_T, ϕ, η (pseudo-rapidity), and particle identity (e.g. π, K, p, $\bar{p}$, Λ, Σ, Ξ, Ω, ϕ, J/ψ, D, etc.) to all hadrons coming out of the collision region, as well as to electrons, photons, and in restricted circumstances (i.e. high rapidity) muons.

  Exercise 2 (Particle data) *What are the masses, lifetimes, and most interesting quantum numbers of the particles mentioned above? How far does a D^+ meson propagate if it has $E = 3\,\mathrm{GeV}$?* Answer □

- In reality, acceptance in η and ϕ varies: e.g. STAR accepts $|\eta| < 1$, while PHENIX accepts $|\eta| < 0.35$ with incomplete ϕ coverage.

  Exercise 3 (Pseudorapidity) *Pseudorapidity η is defined through $\tanh\eta = \cos\theta$, where θ is the angle relative to the beamline. What is the θ acceptance of PHENIX? The forward muon detectors on PHENIX cover $1.4 < \eta < 2.4$. What range of θ is this?* Answer □

  Exercise 4 (Rapidity) *Rapidity y is defined any given particle as $\tanh^{-1} p_z/E$, where p_z is along the beamline. Show that $y \approx \eta$ for large p_z, and show that $y \to y + \mathrm{const}$ on Lorentz boosts in the z direction.* Answer □

- Most particles come out with $p_T < 1\,\mathrm{GeV}$. The high-momentum tails reach up to $p_T \sim 8$ to $10\,\mathrm{GeV}$.

2.2. The quark-gluon plasma

400 nucleons go in, 7500 come out. So a lot of entropy gets produced. A more non-trivial claim is that a thermalized quark-gluon plasma is formed with T as high

as $300\,\mathrm{MeV}$, which then cools isentropically and then hadronizes.

Part of the evidence for a thermalized QGP is:

- Hadron yields at mid-rapidity can be fit to a thermal model (i.e. Bose-Einstein or Fermi-Dirac occupation numbers): even multi-strange hadrons fit. See figure 2.
- Rapidity distributions of protons tend to show that $28 \pm 3\,\mathrm{TeV}$ of the total $39\,\mathrm{TeV}$ of energy winds up in heating the newly created medium (putatively the QGP) and in its collective motion [8].

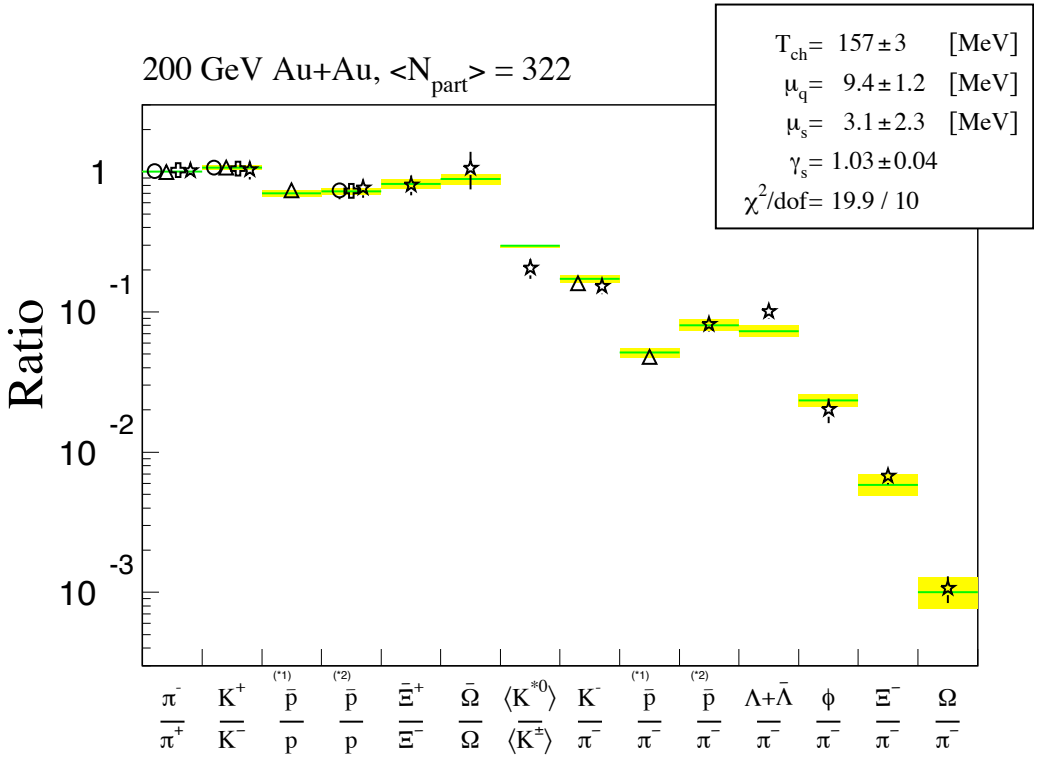

Figure 2: *Ratios of hadron yields observed near mid-rapidity. The lines are the predictions of the thermal model. From [7]. Note that the chemical potentials for light quarks and strange quarks are* small *compared to the temperature.*

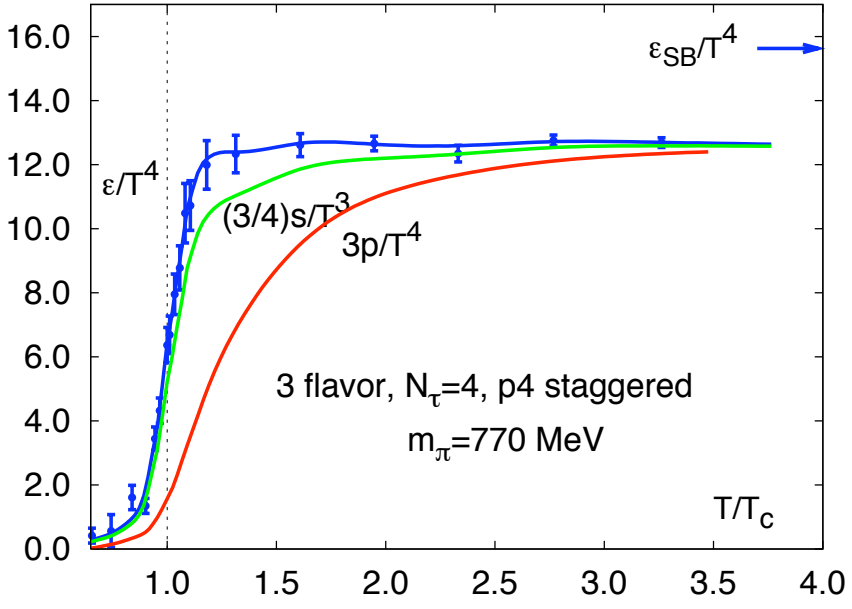

Figure 3: *Lattice results for the equation of state of QCD. From [9].*

- Lattice calculations show that deconfinement happens at $T_c \approx 170\,\mathrm{MeV}$, and that ϵ/T^4 has a plateaux at 80% of the free field value as far above T_c as lattice calculations can reach: see figure 3. Deconfinement and chiral symmetry restoration happen via a smooth but rapid cross-over.

$$\epsilon \approx 6.3\,\mathrm{GeV/fm}^3 \left(\frac{T}{250\,\mathrm{MeV}}\right)^4 \tag{1}$$

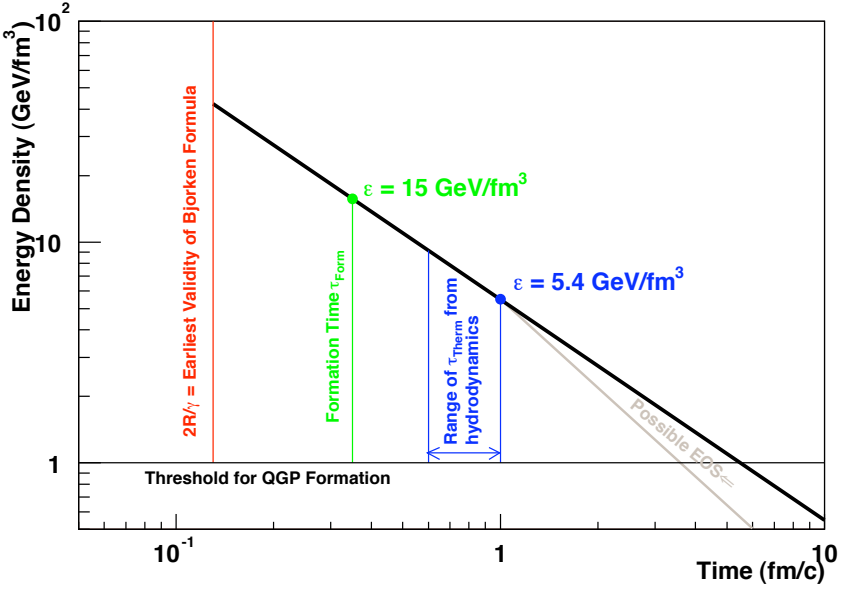

Figure 4: *Energy density as a function of time in a central gold-gold collision, according to an elaboration of the phenomenological Bjorken model. From [3].*

- Simple phenomenological models (with some support from experiment) indicate that energy densities in gold-gold collisions may reach $30\,\mathrm{GeV/fm^3}$ and thermalize by the time $\epsilon \sim 5\text{-}9\,\mathrm{GeV/fm^3}$ [3]—well above the QGP threshhold of $1\,\mathrm{GeV/fm^3}$: see figure 4.

Exercise 5 ($\mathbf{Z}_2$ lattice gauge theory) *Lattice gauge theory is too often viewed as a black box by non-practitioners. Let's "open the box" with the simplest possible gauge theory example: Wegner's $\mathbf{Z}_2$ gauge theory [10], defined on a square $2-d$ lattice. Each link carries a sign s_i, and the action and partition function are*

$$H = -\sum_p \prod_{i=1}^{4} s_{p_i} \qquad Z = \sum_{s_i=\pm 1} e^{-\beta H}, \tag{2}$$

where the sum in H over all plaquettes p and the product inside that sum is over the four links p_1 through p_4 bordering the plaquette. Wegner considered analogs of Wilson operators:

$$W_\gamma = \prod_{i=1}^{\text{length } \gamma} s_{\gamma_i} \tag{3}$$

where γ is a closed path on the lattice.

What is the gauge invariance of (2) and (3)? Convince yourself that $\langle W_\gamma \rangle$ exhibits a perimeter law at low T and an area law at high T. (Yes, this is backward from QCD expectations.) (Hint: it helps to expand $e^{\pm}\beta = \cosh\beta(1 \pm \tanh\beta)$.) Answer □

2.3. Centrality, elliptic flow, and jet-quenching

A *central collision* is one where the gold nuclei hit head-on. A peripheral collision is one where they almost missed. How to quantify this?

- There is (at least at PHENIX and STAR) an event-by-event determination of centrality as well as the reaction plane defined by the beam line and the impact parameter.

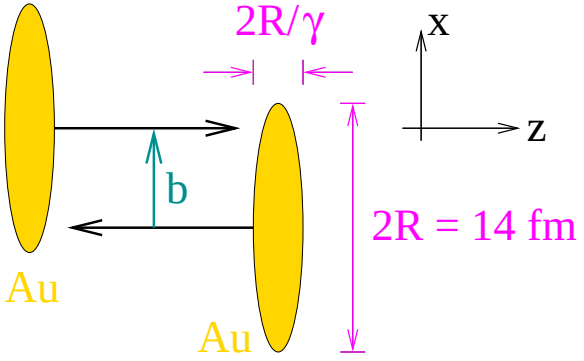

Figure 5: *A gold-gold collision of intermediate centrality. The reaction plane is the plane of the page, in which the centers of mass of both gold nuclei are assumed to lie.*

- In other words, they measure $\vec{b}$ as a vector. See figure 5.
- Centrality refers to the percentage of the total cross-section: i.e. the 10% of all events that have the smallest values of b are described as having central of 0 to 10%.
- In the sphere-overlap model of the inelastic cross-section (which is crude), the impact parameter corresponding to 10% centrality is evaluated like this [11]:

$$0.1\ \sigma_{\rm tot} = \int_0^{b_{10}} dr\ 2\pi r \qquad \text{so} \qquad b_{10} = 2R\sqrt{0.1}\,. \tag{4}$$

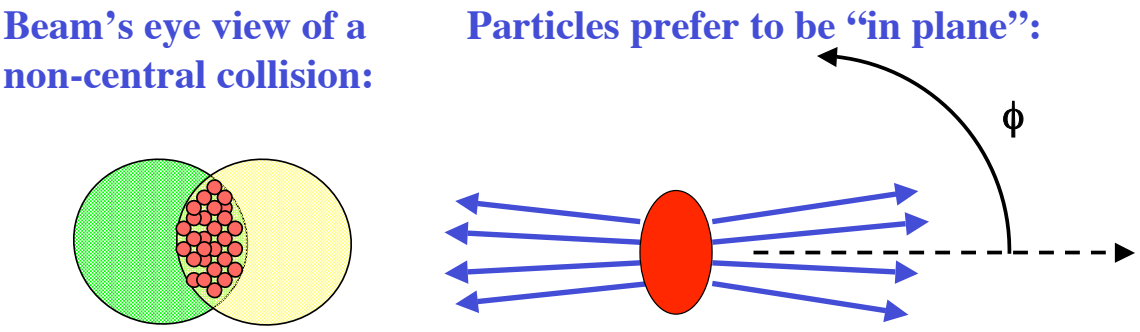

Figure 6: *Cartoon of elliptic flow. From [12].*

Elliptic flow occurs in non-central collisions. In the sphere overlap model, the overlap region is roughly ellipsoidal with all axes unequal (biggest in y, smallest in z). The distribution of observed particles is parametrized as

$$\frac{dN}{p_T dp_T dy d\phi}(p_T, y, \phi; b) = \frac{dN}{p_T dp_T dy}\left[1 + 2v_2(p_T, y; b)\cos 2\phi + \ldots\right], \qquad (5)$$

And v_2 is measured for different particle species. $\phi = 0$ means emission in the reaction plane, so $v_2 > 0$ means this is preferred.

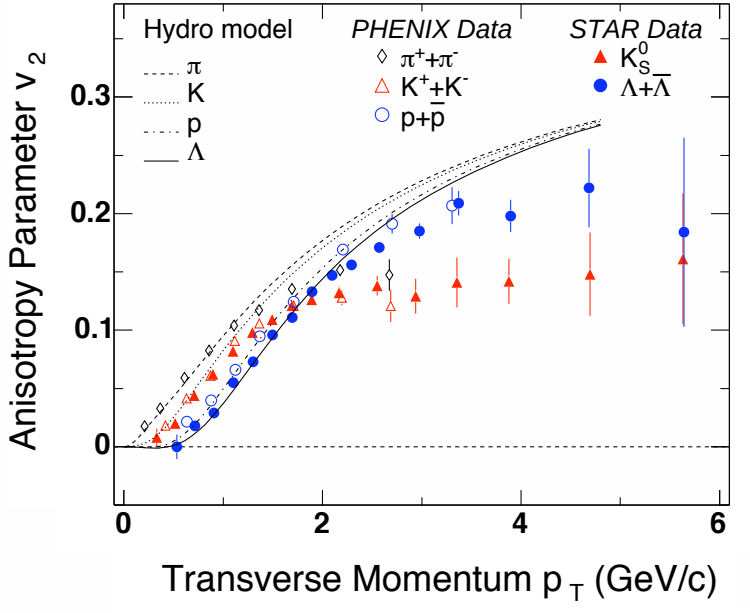

Figure 7: v_2 *near mid-rapidity, with hydrodynamic calculations shown as dashed lines. From [1].*

Sizable observed values of v_2 are in line with hydrodynamic models of *collective flow*:

$$\frac{D}{Dt}(\epsilon\vec{v}) = -\nabla P \tag{6}$$

with ∇P bigger at $\phi = 0$ than $\phi = \pi/2$ because the ellipsoid is shorter at $\phi = 0$ and longest at $\phi = \pi/2$.

Jet-quenching refers to the rapid loss of energy of a hard parton propagating through the hot dense matter created in a gold-gold collision. The prima facie evidence for jet quenching is the the suppression of high p_T jets (more precisely, high p_T hadrons) relative to expectations from "binary collsion scaling."

- Jet production from proton-proton collisions is well studied, as is photon production.
- Binary scaling means to multiply yields in proton-proton by the ratio of incident parton flux of a gold-gold collision to the analogous flux for proton-proton.
- This scaling basically works for high-energy photons ($2\,\mathrm{GeV}/c < p_T < 14\,\mathrm{GeV}/c$) [13].
- It doesn't work for high p_T hadrons: at mid-rapidity,

$$R_{AA} \equiv \frac{dN(\text{gold-gold})/dp_T d\eta}{\langle N_{\text{binary}}\rangle dN(\text{proton-proton})/dp_T d\eta} \approx 0.2 \tag{7}$$

  where $\langle N_{\text{binary}}\rangle$ is the number of nucleon-nucleon collisions in a "factorized" gold-gold collision.

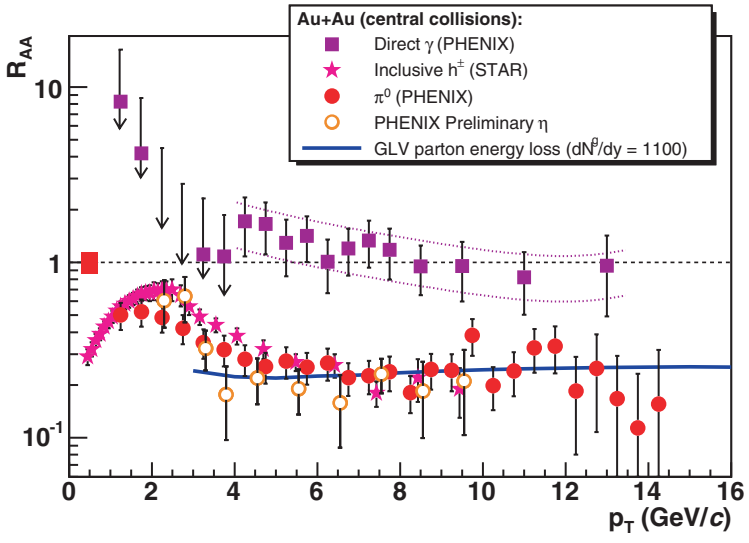

Figure 8: *Nuclear modification factor R_{AA} for photons and hadrons in 0 to 10% central gold-gold collisions.*

2.4. Summary of experiment

In central gold-gold collisions with $200\,\mathrm{GeV}$ per nucleon center-of-mass energy, a thermalized QGP forms as early as $t \sim 0.6\,\mathrm{fm}/c$ with T as high as $300\,\mathrm{MeV}$. It expands and cools isentropically with $\epsilon \propto 1/t$ (or maybe $1/t^{4/3}$) and hadronizes at about $t \sim 6\,\mathrm{fm}/c$.

Sizable anisotropy v_2 indicates elliptic flow of the QGP: a collective hydrodynamic motion which can be successfully modeled via inviscid hydro. Significant viscosity spoils the agreement: $\eta/s \ll \hbar$ seems to be a consensus from RHIC.

Measurements of R_{AA} show that the QGP is approximately transparent to high-energy photons, but remarkably opaque to hadrons.

Lattice does well with equation of state, but transport properties, e.g. v_2 and R_{AA}, are hard. $N = 3$ and $g_{YM}^2 N \sim 10$, so maybe we can make progress with AdS/CFT.

3. AdS/CFT primer

Near-extremal D3-branes are 10-dimensional generalizations of the Reissner-Nordstrom solution for charged black holes. They encode the finite-temperature dynamics of $\mathcal{N} = 4$ super-Yang-Mills theory in $3 + 1$ dimensions and offer an "analogous system" to the QGP over which we have good analytical control at large N and large $g_{YM}^2 N$.

3.1. Near-extremal D3-branes

All calculations discussed here start with type IIB string theory at low energies, plus classical extended strings. The relevant part of the action is

$$S = \frac{1}{2\hat{\kappa}^2} \int d^{10}x \sqrt{\hat{G}} \left[\hat{R} - \frac{1}{4}\hat{F}_5^2 - \frac{1}{2}(\partial\hat{\phi})^2 \right] - \frac{1}{2\pi\alpha'} \int d^2\sigma \, e^{\hat{\phi}/2} \sqrt{\hat{g}} \, . \qquad (8)$$

A few "elementary" points to remember:

- $\hat{F}_5 = *\hat{F}_5$ is imposed after other equations of motion are derived.
- $g_{\alpha\beta} = \partial_\alpha X^M \partial_\beta X^N \hat{G}_{MN}$ is the induced metric on the worldsheet.
- $e^{\hat{\phi}/2}$ arises because $\hat{G}_{MN}$ is the Einstein metric.

- Hatted quantities like $d\hat{s}^2$ and $\hat{\kappa}^2$ are ten-dimensional. Soon we will switch to five-dimensional quantities like ds^2 and κ^2.

The near-horizon geometry of near-extremal D3-branes is

$$d\hat{s}^2 = \frac{L^2}{z^2}\left(-h dt^2 + d\vec{x}^2 + \frac{dz^2}{h}\right) + L^2 d\Omega_5^2 \qquad h = 1 - (z/z_H)^4 \,. \tag{9}$$

Exercise 6 (Near-horizon solution) *Show that this is a solution to the equations of motion (8) with constant dilaton. What is the appropriate $\hat{F}_5$?* Answer □

Standard arguments lead to

$$L^4 = \frac{\hat{\kappa} N}{2\pi^{5/2}} = g_{YM}^2 N \alpha'^2 \qquad T = \frac{1}{\pi z_H} \,. \tag{10}$$

The horizon across a coordinate volume V_3 in the $\vec{x}$ directions is proportional to the entropy of the gauge theory in the same volume [14]:

$$\begin{aligned} A_H &= V_3 \frac{L^3}{z_H^3} \pi^3 L^5 = V_3 T^3 L^8 \pi^6 \\ s &= \frac{S}{V_3} = \frac{A_H}{V_3 \hat{\kappa}^2/2\pi} = \frac{\pi^2}{2} N^2 T^3 \,. \end{aligned} \tag{11}$$

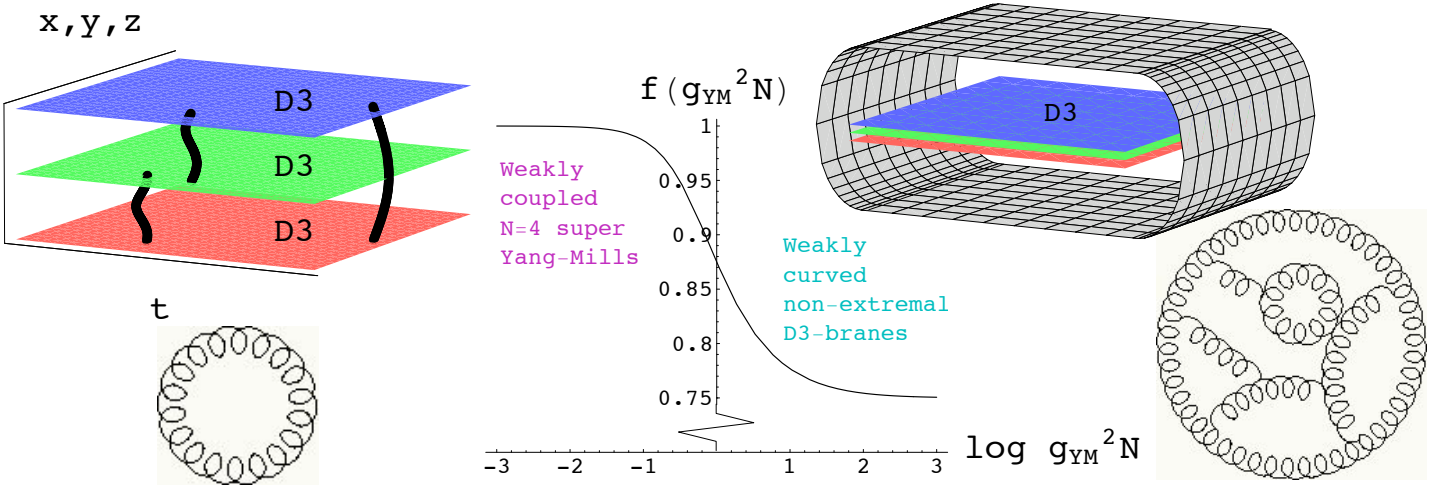

Figure 9: *An* ad hoc *interpolation between weak and strong coupling expressions for the entropy,* $s = s_{\rm free} f(g_{YM}^2 N)$. *At large* $g_{YM}^2 N$, *the classical horizon "resums" arbitrarily large Feynman diagrams.*

This is 75% of the free field value

$$s = \frac{2\pi^2}{3} N^2 T^3 \,. \tag{12}$$

Exercise 7 (Entropy density comparison) *Compare* s *for* $SU(3)$ $\mathcal{N} = 4$ *gauge theory at zero coupling with* s *for QCD with three flavors at zero coupling.* Answer □

It is striking that the deficit in (11) is numerically similar to the 80% deficit from lattice QCD (see figure 3). Could such behavior be universal for large $g_{YM}^2 N$?

3.2. A universal graviton absorption calculation

The relevance of strings to RHIC started to seem possible because of a computation [15] for near-extremal D3-branes:

$$\frac{\eta}{s} = \frac{\hbar}{4\pi} \,. \tag{13}$$

This dovetails better with the "experimentally observed" range $0 \leq \eta/s \ll 1$ than other first-principles calculations: for example, if $\lambda = g_{YM}^2 N$ is small, then

$$\frac{\eta}{s} \sim \frac{1}{\lambda^2 \log 1/\lambda} \gg 1 \,. \tag{14}$$

Additional interest attaches to (13) because it saturates a conjectured viscosity bound $\eta/s \geq \hbar/4\pi$ [16] to which there are no known exceptions.

The calculation leading to (13) hinges on graviton absorption by branes. See figure 10.

$$S_{\text{D3-brane}} \supset \int d^4x \, h_{\mu\nu} T_{\mu\nu} \,. \tag{15}$$

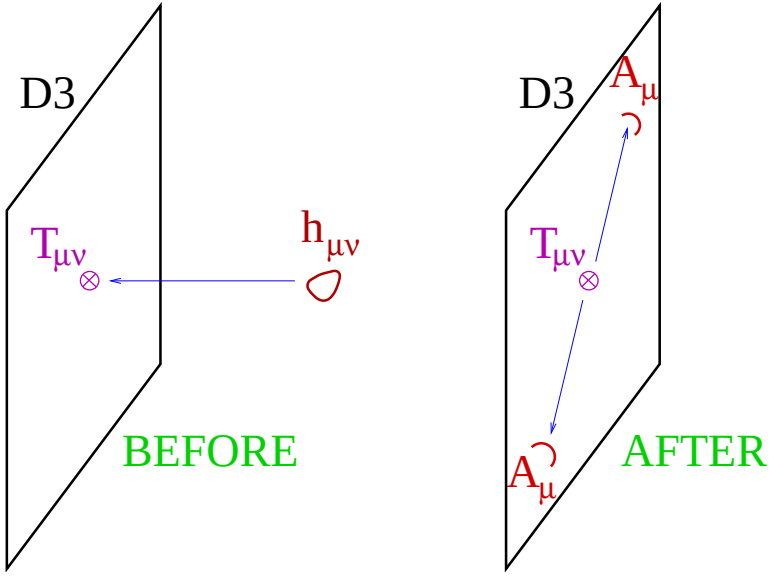

Figure 10: *A graviton (shown as a massless closed string) splits into gauge quanta (shown as open strings) upon colliding with the brane.*

The cross-section for absorption of a graviton h_{xy}, from the coupling (15), is

$$\sigma(\omega) = V_3 \frac{8\pi G_N}{\omega} \int d^4x\, e^{i\omega t} \langle [T_{xy}(t,\vec{x}), T_{xy}(0)] \rangle \,. \tag{16}$$

The factor of V_3 is because the D3-brane is extended: V_3 is its (infinite) 3-volume in the $\vec{x}$ directions.

But in the gravitational picture where the D3-brane has a horizon, the graviton has some classical cross-section to fall into it. It turns out that

$$\sigma(\omega) \to A_{\text{horizon}} = 4G_N S \qquad \text{as } \omega \to 0\,. \tag{17}$$

Conveniently, the viscosity is

$$\begin{aligned} \eta &= \lim_{\omega\to 0} \frac{1}{2\omega} \int d^4x\, e^{i\omega t} \langle [T_{xy}(t,\vec{x}), T_{xy}(0)] \rangle \\ &= \frac{\sigma(0)}{16\pi G_N V_3} = \frac{s}{4\pi}\,. \end{aligned} \tag{18}$$

So we've verified (13). The key step is (17). An old result [17], refreshed and extended in [18], says that (17) is always true for backgrounds of two-derivative supergravity.

- The basic idea: spin-two gravitons decouple from matter fields in backgrounds of interest and so satisfy Klein-Gordon equation in dimensions transverse to the brane.

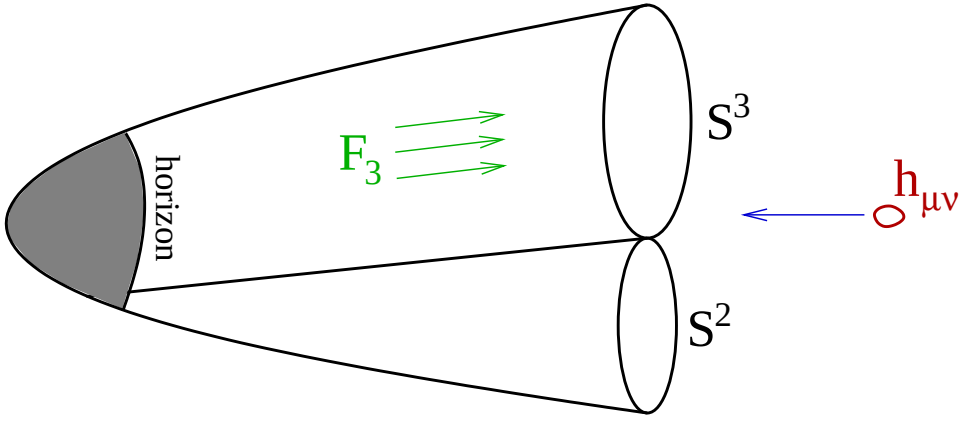

Figure 11: *A more complicated transverse geometry (related to the duality cascades discussed by I. Klebanov at this school) does not affect the propagation of gravitons* h_{xy}.

- All the complications of the relevant supergravity geometries are in directions *orthogonal* to indices of $h_{\mu\nu}$. See figure 11.

But higher-derivative terms (finite λ corrections) *do* affect η/s, and the first of these for D3-branes (from $\alpha'^3 R^4$) makes $\eta/s > 1/4\pi$ [16].

The smallness of η/s is now proposed by some RHIC physicists as a measure of strong coupling [1].

Exercise 8 (Estimating viscosity) *Show that* $\eta \sim \epsilon\, \tau_{\rm MFP}$ *where* $\tau_{\rm MFP}$ *is the mean free time.*

Answer □

3.3. Don't bring out the champagne just yet

The combination of the entropy deficit (11) and the viscosity calculation (13) has drawn the attention of RHIC phenomenologists. DOE higher-ups also seem to have heard that something interesting is afoot:

> "The possibility of a connection between string theory and RHIC collisions is unexpected and exhilarating." (R. Orbach [19])

The excitement is merited! But let's not forget that $\mathcal{N} = 4$ gauge theory misses several essential features of QCD:

- No confinement. Coupling doesn't run: it's a parameter you can dial.

  But is this so bad? We want to use AdS/CFT at finite temperature to model the QGP above T_c. Phenomenological studies of RHIC physics routinely set $v_s = 1/\sqrt{3}$ and $\epsilon \sim 1/t^{4/3}$ (both corresponding to conformal invariance) for the QGP, e.g. when ϵ is significantly above $1\,\mathrm{GeV}$.

- No chiral condensate.

  But is this so bad? The chiral condensate turns off around T_c according to lattice calculations.

- All fundamental matter fields are in adjoint representation: A_μ, four Majorana fermions λ_i, six real scalars X_I.

This looks kind of bad. Maybe gauge interactions dominate the dynamics anyway?

Variants on the D3-brane construction exist which exhibit confinement, but there's often two funny things about them:

1. Confinement scale is essentially identical to a flavor physics scale. An example helps:

$$\mathcal{L}_{\text{soft}} = -\frac{1}{2}\sum_{I=1}^{6} m^2 |X_I|^2 - \frac{1}{2}\sum_{i=1}^{3} m\bar{\lambda}_i\lambda_i \tag{19}$$

leads to $\beta(g) < 0$; get

$$\Lambda_{\text{confine}} \sim m e^{-8\pi^2/\lambda(m)} \approx m \tag{20}$$

because $\lambda(m)$ is large. It's a bit like having a bunch of copies of the s quark, such that above m_s the beta-function (almost) vanishes (but λ is still big). You wind up studying analogs of flavor physics as much as confinement itself.

2. The QCD string tension is often much bigger than the mass gap,

$$\tau_{\text{QCD string}}/m_{\text{gap}}^2 \sim \sqrt{g_{YM}^2 N}\,. \tag{21}$$

Roughly, this arises because $m_{\text{gap}}^2 \sim g_{tt}^*/L$, but $\tau \sim g_{tt}^*/2\pi\alpha'$. See figure 12.

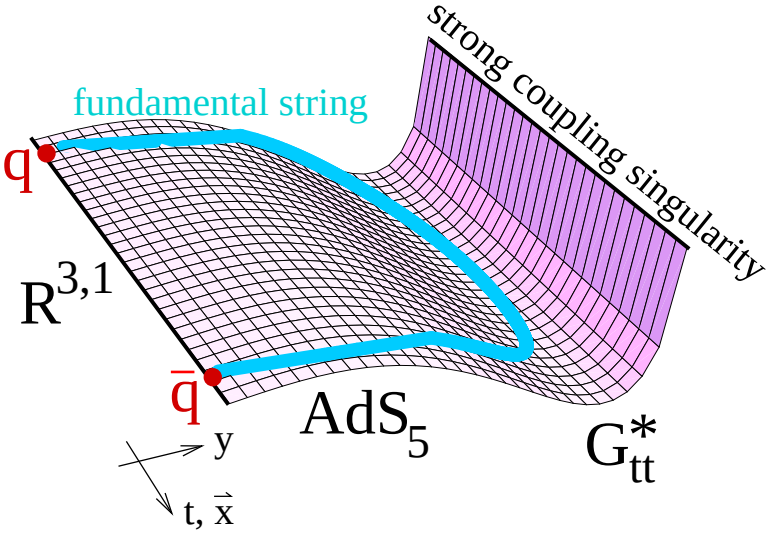

Figure 12: *The QCD string in a simple confining variant of AdS_5 produced by a dilaton gradient plus back-reaction [20].*

We have to ask more of string theory before we can expect broad agreement with QCD.

Still, the worst problems relate to the vacuum, so comparisons with RHIC are probably the best hope to date. It should also encourage us that lattice methods has trouble (at present) in delivering reliable characterizations of transport phenomena.

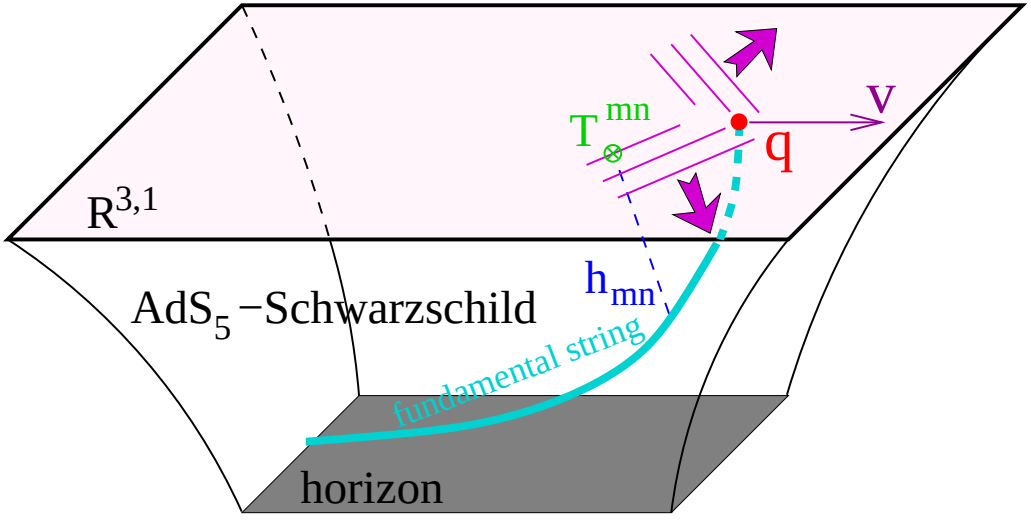

Figure 13: *In blue: the trailing string of an external quark, following [21, 22]. The dashed line shows classical propagation of a graviton from the string to the boundary, where its behavior can be translated into the stress-energy tensor $\langle T_{mn} \rangle$ of the boundary gauge theory [23].*

4. Jet-quenching and trailing strings

An analog of jet-quenching in AdS/CFT should involve a colored probe that we drag through the QGP, preferably at relativistic speeds. Readiest to hand are external quarks: strings with one end on the boundary. See figure 13.

The trailing string exerts a drag force [21, 22]:

$$\frac{dp}{dt} = -\frac{\pi\sqrt{g_{YM}^2 N}}{2} T^2 \frac{v}{\sqrt{1-v^2}} \tag{22}$$

on the quark.

The stress tensor $\langle T_{mn} \rangle$ produced in the boundary gauge theory exhibits broadly peaked high-angle emission that seems to qualitatively match recent results from RHIC [24] on away-side jet splitting.

4.1. Preliminaries

At $T = 0$, $\mathcal{N} = 4$ super-Yang-Mills has a moduli space of degenerate vacua corresponding to separating D3-branes. Strings between different D3-branes are analogs of W-bosons, where the mass comes from the Higgs mechanism. See figure 14b.

If we split one brane off from a great many others, a slight idealization is to regard it as a test brane in AdS_5 at fixed $z = z_*$. The mass of a static string attached to the test brane is

$$m_{\text{static}} = \frac{1}{2\pi\alpha'} \frac{L^2}{z_*}, \tag{23}$$

which can be shown to agree with the tree-level Higgs mass. (This agreement be-

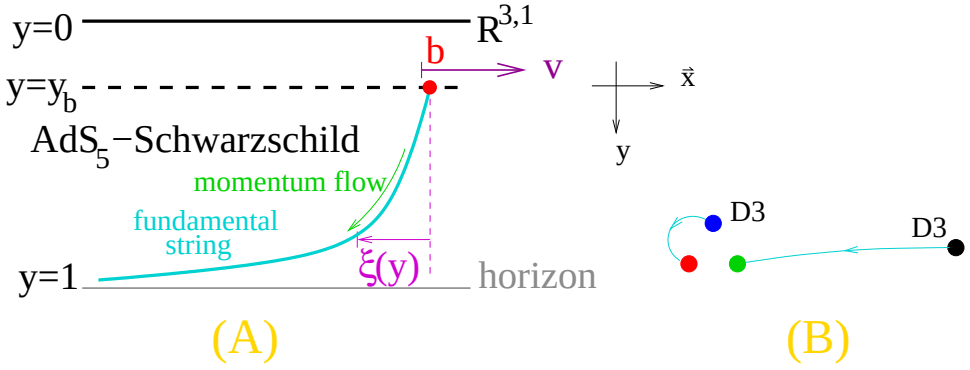

Figure 14: *(A) A finite mass quark moving at velocity v through the QGP can be represented as a string hanging from a "flavor brane" [21]. This picture is best justified for heavy quarks like c and b. In this figure and below, we use the radial coordinate $y = z/z_H$. (B) At $T = 0$, flavor branes can be realized by separating one D3-brane from several others. The massive W boson is similar to a heavy quark. We also show a $R\overline{B}$ gluon.*

tween strong coupling and tree level is an example of supersymmetric non-renormalization of BPS quantities.)

At $T \neq 0$, the separated branes attract because the moduli get thermal masses. But other string theory constructions exist which provide for finite mass quarks at $T \neq 0$: see figure 14 and the discussion of D7-branes in [21].

Regardless of its 10-dimensional origin, the flavor brane at $z = z_*$ serves as a useful UV regulator. The mass of a static string hanging from the flavor brane into the

horizon is

$$m_{\text{static}} = \frac{L^2}{2\pi\alpha'}\left(\frac{1}{z_*} - \frac{1}{z_H}\right) = \frac{\sqrt{g_{YM}^2 N}}{2} T \left(\frac{z_H}{z_*} - 1\right)$$
$$\frac{z_H}{z_*} = 1 + \frac{2}{\sqrt{g_{YM}^2 N}} \frac{m_{\text{static}}}{T} \,. \tag{24}$$

Pitfalls of applying (24) naively to quarks whose mass is comparable to T were discussed in [21]. Despite these potential difficulties, we will use the flavor brane picture to represent both heavy and light quarks.

Lattice calculations show that light quarks acquire thermal masses proportional to T. Charm and beauty are rather more massive because of electroweak Higgs. To be definite, let's use the values in table 1, as well as

$$g_{YM}^2 N = 10 \qquad T = \frac{1}{\pi}\,\text{GeV} \approx 318\,\text{MeV}\,. \tag{25}$$

quark	mass/MeV	z_*/z_H
u,d,s	300	0.63
c	1400	0.26
b	4800	0.09

Table 1: *A rough assignment of quark masses appropriate to a thermal plasma at* $T = 318\,\mathrm{MeV}$ *with* $g^2_{YM}N = 10$.

Exercise 9 (Mass of a static string) *Verify (23) and (24). Integrate the equation for* E_3 *in (56) in the limit* $v \to 0$, $\vec{K} \to 0$, *and use (61), and (60) to reproduce (24). It helps to know that* $Q^{\rm tot}_{E_1} + 2Q^{\rm tot}_{E_3} = 0$.

Answer □

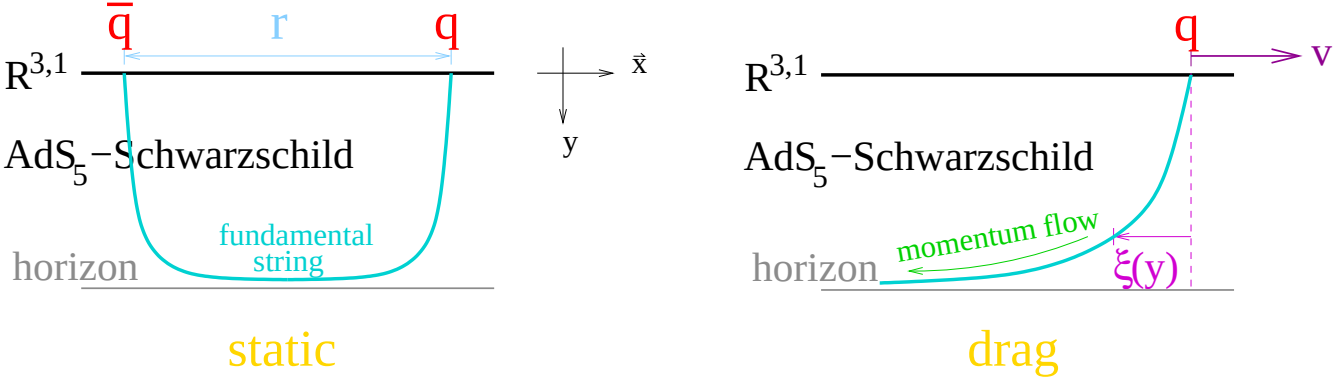

Figure 15: *Static force versus drag force.*

4.2. A drag force computation

$G_{tt} \propto 1 - z^4/z_H^4 \to 0$ at the horizon of AdS-Schwarzschild, so the *static force* between quarks goes to zero as separation increases. But *drag force* on a moving quark is finite. See figure 15. We need to know the shape of the trailing string and the momentum flow down it. We assume a "co-moving" ansatz:

$$x^1(t, y) = vt + \xi(y) \tag{26}$$

where $y = z/z_H$, so that AdS_5-Schwarzschild takes the form

$$ds^2 = \frac{L^2}{z_H^2 y^2}\left(-h dt^2 + d\vec{x}^2 + z_H^2 \frac{dy^2}{h}\right) \qquad \boxed{h \equiv 1 - y^4} \qquad z_H = \frac{1}{\pi T} \tag{27}$$

The classical string EOM's are precisely the conservation of worldsheet current of spacetime energy-momentum.

$$S = -\frac{1}{2\pi\alpha'}\int d^2\sigma\, e^{\phi/2}\sqrt{-\det g_{\alpha\beta}} \qquad g_{\alpha\beta} \equiv G_{\mu\nu}\partial_\alpha X^\mu \partial_\beta X^\nu$$
$$\nabla_\alpha P^\alpha{}_\mu = 0 \qquad P^\alpha{}_\mu \equiv -\frac{1}{2\pi\alpha'} G_{\mu\nu}\partial^\alpha X^\nu \tag{28}$$

A differential equation for ξ follows from a "reduced" lagrangian:

$$S = -\frac{L^2 z_H}{2\pi\alpha'}\int dt dy\, \mathcal{L} \qquad \mathcal{L} = -\frac{1}{z_H^2 y^2}\sqrt{1 + \frac{h\xi'^2}{z_H^2} - \frac{v^2}{h}} \tag{29}$$

Conservation of the "momentum" $\pi_\xi \equiv \partial\mathcal{L}/\partial\xi'$ leads to

$$\xi' = \pm\pi_\xi \frac{z_H y^2}{h}\sqrt{\frac{h - v^2}{h - \pi_\xi^2 y^4}}\,. \tag{30}$$

Because ξ' is always real, we have to choose π_ξ to render the right hand side real:

$$\pi_\xi^2 = \frac{v^2}{1-v^2} \qquad \frac{h-v^2}{h-\pi_\xi^2 y^4} = 1 - v^2 \,. \tag{31}$$

This leads to

$$\xi' = -\frac{v z_H y^2}{1-y^4} \qquad \xi = -\frac{v z_H}{4i}\left(\log\frac{1-iy}{1+iy} + i\log\frac{1+y}{1-y}\right) \,. \tag{32}$$

It looks like we could also have chosen $\pi_\xi = 0$, corresponding to $\xi = 0$: a straight moving string! But $\mathcal{L}$ becomes imaginary for $y > y_v = \sqrt[4]{1-y^4}$, and the parts of the string for $y > y_v$ are moving on spacelike trajectories (i.e. faster than light).

Several works [25, 26, 27] have elucidated the meaning of y_v: intuitively, in the rest frame of the moving quark, there is a "boundary layer" for small y where the string doesn't feel any drag. Below that boundary layer it "catches in the hot wind" and blows back into the shape (32). In gauge theory terms, this means that objects smaller than a certain velocity-dependent radius can propagate almost without drag.

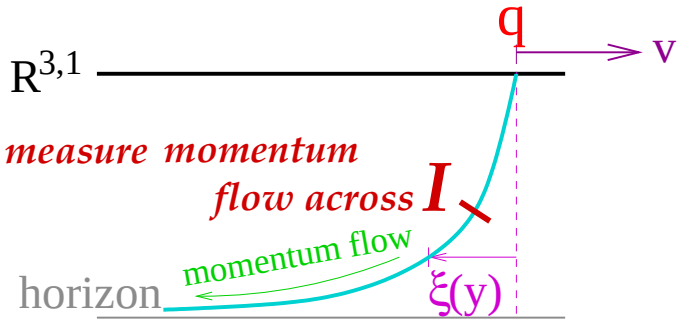

Figure 16: *The drag force is computed by measuring the momentum flux down the string. The position of $\mathcal{I}$ is arbitrary because the energy-momentum current is conserved.*

Momentum and energy drains down the string: see figure 16.

$$\Delta P_1 = -\int_{\mathcal{I}} dt\, \sqrt{-g} P^y{}_{x^1} = \frac{dp_1}{dt}\Delta t\,. \tag{33}$$

dp_1/dt is precisely the drag force:

$$F \equiv \frac{dp}{dt} = -\frac{\pi\sqrt{g_{YM}^2 N}}{2}\frac{v}{\sqrt{1-v^2}}\,. \tag{34}$$

The result (34) holds unaltered if we have the strings end on a flavor brane at $y = y_* = z_*/z_H$: the trailing string has exactly the shape (32) for $y_* < y < 1$. *Provided* $m = m_{\text{static}} \gg T$, we can use standard relativistic expressions like $E = \sqrt{p^2 + m^2}$

and $p = mv/\sqrt{1-v^2}$. Then (34) becomes

$$F = -\frac{p}{t_0} \qquad t_0 = \frac{2}{\pi\sqrt{g_{YM}^2 N}}\frac{m}{T^2}\,. \tag{35}$$

A detailed discussion of modified dispersion relations $E = E(p)$ derived from the hanging string picture can be found in [21].

Let's rewrite (35) in a form suggestive of comparison to real-world heavy quarks:

$$\begin{aligned} \text{beauty:} \qquad & t_0 \approx 1.9\,\mathrm{fm}/c\,\frac{m/(4800\,\mathrm{MeV})}{\sqrt{g_{YM}^2 N/10}\,(T/318\,\mathrm{MeV})^2} \\ \text{charm:} \qquad & t_0 \approx 0.6\,\mathrm{fm}/c\,\frac{m/(1600\,\mathrm{MeV})}{\sqrt{g_{YM}^2 N/10}\,(T/318\,\mathrm{MeV})^2}\,. \end{aligned} \tag{36}$$

For light quarks, the dispersion relation issues render (35) less well justified, but perhaps we are justified in estimating $t_0 \lesssim 0.3\,\mathrm{fm}/c$.

These are interesting numbers because they indicate that charm has a stopping length that is small compared to the extent of the QGP.

- So it makes sense that charm participates in the QGP's collective motion: briefly, "charm flows."

- The experimental evidence for this comes from measuring the ϕ distribution of electrons with energies typical of $D \to K + e + \nu$ decays.
- "A large contribution to the flow must come from interactions in the first $2\,\mathrm{fm}/c$ after the collision" [1].
- "The elliptic flow is generated mainly during the first $5\,\mathrm{fm}/c$ of the expansion" [1].
- So is QGP hot enough for long enough to affect b's somewhat? The current consensus seems to be NO, but I am unaware of the experimental evidence.

Exercise 10 (Stopping length) *As a dimensionless figure of merit describing how many stopping lengths of QGP a quark travels through, consider*

$$n_{\mathrm{stop}} \equiv \int_{t_i}^{t_f} \frac{dt}{t_0} \tag{37}$$

where t_0 is given by (36). Using Bjorken scaling of the energy density, $\epsilon \propto 1/t$, calculate n_{stop} for both c and b quarks in a central gold-gold collision. Use $\epsilon_i = 5\,\mathrm{GeV/fm}^3$, $t_i = 1\,\mathrm{fm}/c$, and $t_f = 5\,\mathrm{fm}/c$. You may use the approximate formula (1). It may be helpful to refer to figure 4. Answer □

4.3. The wake of a quark

A much-discussed aspect of RHIC's current experimental program hinges on the following picture:

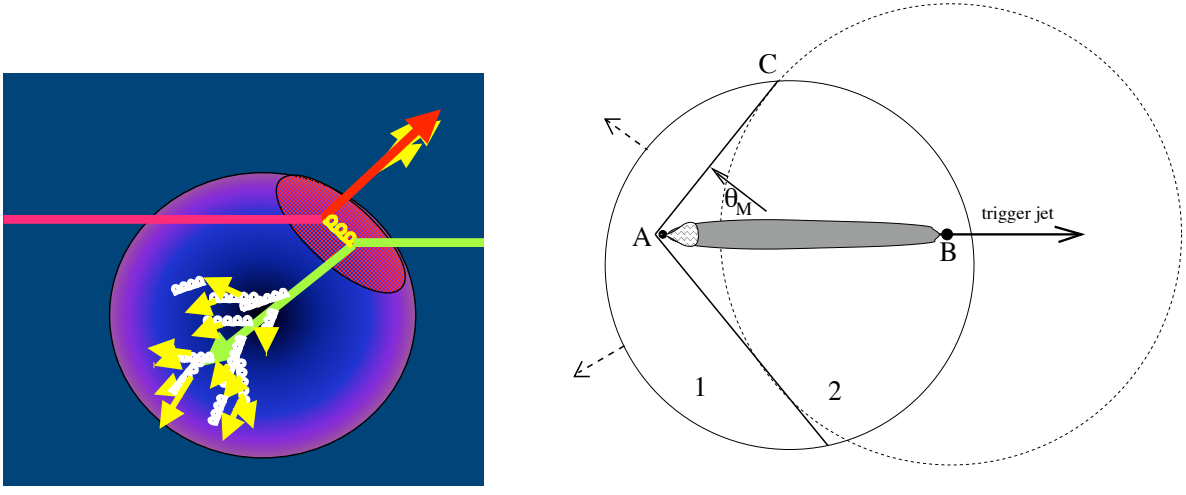

Figure 17: *Left: A di-jet event with significant away-side jet quenching. From [28]. Right: The away-side parton may generate a sonic boom, with* $\theta_M = \cos^{-1}(c_s/v)$ *the Mach angle. From [29].*

- Two hard partons collide near the surface of the QGP.
- One escapes and fragments into the "near side" jet.
- The other plows through the QGP and dissipates a lot of energy.
- Such events give us a hard probe of the QGP: "jet tomography."
- All the low p_T junk makes jet reconstruction impractical, so instead one triggers on a high p_T hadron and look at the angular distribution of one or more associated hadrons, also with $p_T > 1\,\mathrm{GeV}$ to get above the backgrounds.

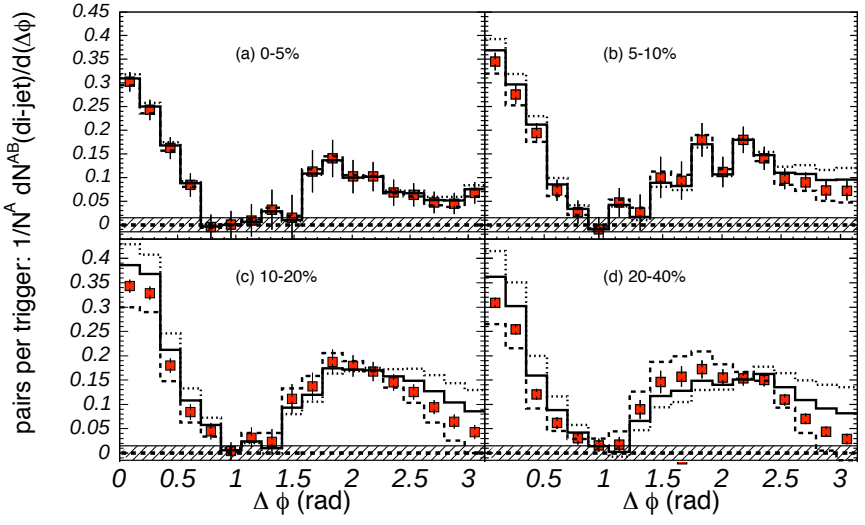

Figure 18: *Histograms of the azimuthal angle between the trigger hadron (with* $2.5\,\mathrm{GeV}/c < p_T < 4\,\mathrm{GeV}/c$*) and the partner hadron (with* $1\,\mathrm{GeV}/c < p_T < 2.5\,\mathrm{GeV}/c$*) for different centralities. Away-side jet splitting, illustrated by the broad peak around* $\Delta\phi = 2$*, is evidence for high-angle emission in the QGP. From [24].*

The sonic boom picture and related theoretical proposals (see for example [29, 30, 31, 32, 33]) suggest that high-angle emission carries away a lot of the energy. And data seems to confirm this: see figure 18.

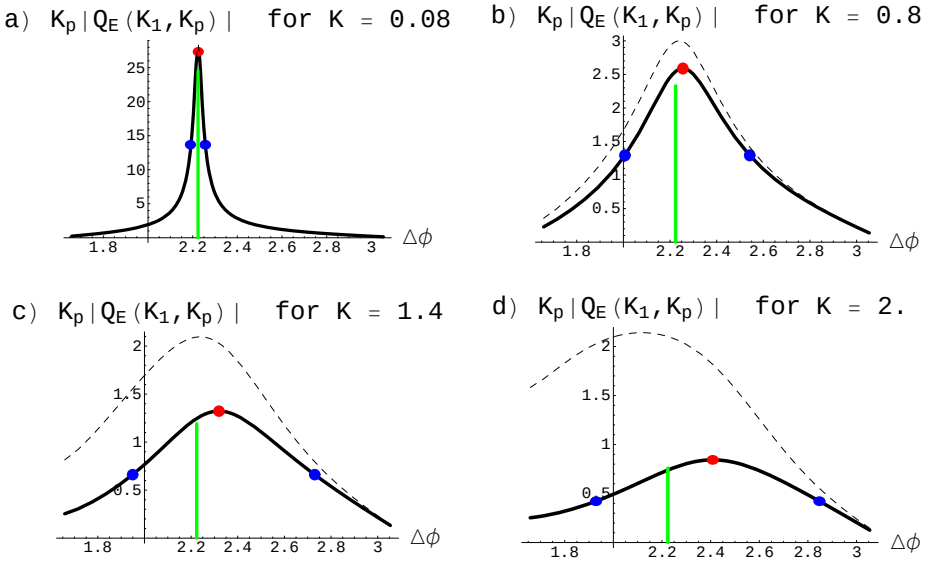

Figure 19: $K_\perp |Q_E^K|$ *at fixed* K *as a function of angle, for* $v = 0.95$. $\Delta\phi = \pi - \theta$ *where* $\theta = \tan^{-1} K_\perp/K_1$. *The dashed lines are from an analytic estimate (67), and the solid lines are from numerics. The green line is the Mach angle; the red dot is the peak; and the blue dots are at half the peak height. Plots (c) and (d) are in the ballpark of the experimental study summarized in figure 18.* K *is the total momentum, in units of* GeV *if* $T = 318\,\mathrm{MeV}$. *For precise definitions of* K, K_1, $K_\perp$, *and* Q_E^K, *see the discussion in section 4.4. From [23].*

It is natural to ask what AdS/CFT has to say about away-side jet splitting. A summary of the results of [34, 23]:

- At low p_T, the trailing string picture provides striking support for emission

peaked near the Mach angle.

- But AdS/CFT calculations are not limited to the infrared limit that best justifies hydrodynamics.
- In a momentum window comparable to experimental studies, e.g. [24], the AdS/CFT calculations show broad peaks at slightly more forward angles than the Mach angle: see figure 19.

The calculations that lead to figure 19 are more intricate than others discussed so far: see section 4.4.

4.4. Graviton perturbations

A good measure of the energy loss is $\langle T_{mn} \rangle$ in the boundary gauge theory. The purpose of this section is to describe the calculation via AdS/CFT of $\langle T_{mn} \rangle$ as concisely as we can without leaving out essential points.

$\langle T_{mn} \rangle$ is determined by the behavior near the boundary of linearized graviton perturbations of AdS_5-Schwarzschild:

$$ds^2_{(0)} = G^{(0)}_{\mu\nu} dx^\mu dx^\nu = \frac{L^2}{z_H^2 y^2} \left(-h dt^2 + d\vec{x}^2 + z_H^2 \frac{dy^2}{h} \right) \qquad h \equiv 1 - y^4 \,. \tag{38}$$

$$G_{\mu\nu} = G^{(0)}_{\mu\nu} + h_{\mu\nu} \,, \tag{39}$$

The Einstein equations are

$$R^{\mu\nu} - \frac{1}{2} G^{\mu\nu} R - \frac{6}{L^2} G^{\mu\nu} = \tau^{\mu\nu} \,, \tag{40}$$

where $\tau^{\mu\nu}$ is the stress-energy of the trailing string.

Even after linearizing (40), we are left with difficult coupled linear PDE's. They can

be attacked by Fourier transforming:

$$h^{\mu\nu}(t,x^1,x^2,x^3,y) = \int \frac{d^3K}{(2\pi)^3}\, h^{\mu\nu}_K(y)\, e^{i\left[K_1(x^1-vt)+K_2x^2+K_3x^3\right]/z_H}\,, \qquad (41)$$

where $\vec{K} = z_H\vec{k} = \vec{k}/\pi T$ is a dimensionless wave-number. Dependence only on $x^1 - vt$ is appropriate for describing the late-time co-moving color fields dual to the trailing string. Schematically the equations take the form

$$\mathcal{E}^{\mu\nu} \equiv \Delta^K_{AdS} h^{\mu\nu}_K - \tau^{\mu\nu}_K = 0\,, \qquad (42)$$

where Δ_{AdS} is an AdS_5-Schwarzschild version of the Lichnerowicz operator. These are still complicated equations, so what next?

- Choose "axial gauge," $h^{\mu y}_K = 0$. Now there are 10 independent quantities h^{mn}_K, where $0 \le m,n \le 3$.
- (42) comprises 10 second order equations of motions, $\mathcal{E}^{mn} = 0$, and five first order constraints, $\mathcal{E}^{\mu y} = 0$.
- The differential equations may be partially decoupled and simplified by making a series of field redefinitions. They are still complicated—see below.
- We have generalized from [23] by allowing the trailing string to end on a flavor

brane at $y = y_*$. This is accomplished simply by including a factor of $\vartheta(y - y_*)$ in $\tau_{\mu\nu}$.

- We take $\vec{K} = (K_1, K_\perp, 0) = K(\cos\theta, \sin\theta, 0)$.

$$h^K_{\mu\nu} = \frac{\kappa^2}{2\pi\alpha'} \frac{1}{\sqrt{1-v^2}} \frac{L}{z_H^2 y^2} \begin{pmatrix} H_{00} & H_{01} & H_{02} & H_{03} & 0 \\ H_{10} & H_{11} & H_{12} & H_{13} & 0 \\ H_{20} & H_{21} & H_{22} & H_{23} & 0 \\ H_{30} & H_{31} & H_{32} & H_{33} & 0 \\ 0 & 0 & 0 & 0 & 0 \end{pmatrix}. \tag{43}$$

$$K = \sqrt{K_1^2 + K_\perp^2} \qquad \theta = \tan^{-1} \frac{K_\perp}{K_1} \tag{44}$$

$$A = \frac{-H_{11} + 2\cot\theta H_{12} - \cot^2\theta H_{22} + \csc^2\theta H_{33}}{2v^2} \tag{45}$$

$$\left[\partial_y^2 + \left(-\frac{3}{y} + \frac{h'}{h}\right)\partial_y + \frac{K^2}{h^2}(v^2\cos^2\theta - h)\right] A = \frac{y}{h} e^{-iK_1\xi/z_H}\vartheta(y - y_*) \tag{46}$$

$$B_1 = \frac{H_{03}}{K^2 v} \qquad B_2 = -\frac{H_{13} + \tan\theta H_{23}}{K^2 v^2} \tag{47}$$

$$\left[\partial_y^2 + \begin{pmatrix} -\frac{3}{y} & 0 \\ 0 & -\frac{3}{y} + \frac{h'}{h} \end{pmatrix}\partial_y + \frac{K^2}{h^2}\begin{pmatrix} -h & v^2\cos^2\theta h \\ -1 & v^2\cos^2\theta \end{pmatrix}\right]\begin{pmatrix} B_1 \\ B_2 \end{pmatrix} = \begin{pmatrix} 0 \\ 0 \end{pmatrix} \tag{48}$$

$$B_1' - hB_2' = 0 \tag{49}$$

$$C = \frac{-\sin\theta H_{13} + \cos\theta H_{23}}{K} \tag{50}$$

$$\left[\partial_y^2 + \left(-\frac{3}{y} + \frac{h'}{h}\right) + \frac{K^2}{h^2}(v^2\cos^2\theta - h)\right] C = 0 \tag{51}$$

$$D_1 = \frac{H_{01} - \cot\theta H_{02}}{2v} \qquad D_2 = \frac{-H_{11} + 2\cot 2\theta H_{12} + H_{22}}{2v^2} \tag{52}$$

$$\left[\partial_y^2+\begin{pmatrix}-\frac{3}{y} & 0\\ 0 & -\frac{3}{y}+\frac{h'}{h}\end{pmatrix}\partial_y+\frac{K^2}{h^2}\begin{pmatrix}-h & v^2\cos^2\theta h\\ -1 & v^2\cos^2\theta\end{pmatrix}\right]\begin{pmatrix}D_1\\ D_2\end{pmatrix}=\frac{y}{h}e^{-iK_1\xi/z_H}\vartheta(y-y_*)\begin{pmatrix}1\\ 1\end{pmatrix} \tag{53}$$

$$D_1'-hD_2'=\frac{y^3}{ivK_1}e^{-iK_1\xi/z_H}\vartheta(y-y_*) \tag{54}$$

$$\begin{gathered}E_1=\frac{1}{2}\left(-\frac{3}{h}H_{00}+H_{11}+H_{22}+H_{33}\right)\qquad E_2=\frac{H_{01}+\tan\theta H_{02}}{2v}\\ E_3=\frac{H_{11}+H_{22}+H_{33}}{2}\qquad E_4=\frac{-H_{11}-H_{22}+3\cos 2\theta(-H_{11}+H_{22})+2H_{33}-6\sin 2\theta H_{12}}{4}\end{gathered} \tag{55}$$

$$\begin{aligned}&\left[\partial_y^2+\begin{pmatrix}-\frac{3}{y}+\frac{3h'}{2h} & 0 & 0 & 0\\ 0 & -\frac{3}{y} & 0 & 0\\ 0 & 0 & -\frac{3}{y}+\frac{h'}{2h} & 0\\ 0 & 0 & 0 & -\frac{3}{y}+\frac{h'}{h}\end{pmatrix}\partial_y\right.\\ &\qquad\left.+\frac{K^2}{3h^2}\begin{pmatrix}-2h & 12v^2\cos^2\theta & 6v^2\cos^2\theta+2h & 0\\ 0 & 0 & 2h & h\\ 0 & 0 & -2h & -h\\ 2h & -12v^2\cos^2\theta & 0 & 3v^2\cos^2\theta+h\end{pmatrix}\right]\begin{pmatrix}E_1\\ E_2\\ E_3\\ E_4\end{pmatrix}\\ &\qquad=\frac{y}{h}e^{-iK_1\xi/z_H}\vartheta(y-y_*)\begin{pmatrix}1+\frac{v^2}{h}\\ 1\\ -1+v^2-\frac{v^2}{h}\\ v^2\frac{1+3\cos 2\theta}{2}\end{pmatrix}\end{aligned} \tag{56}$$

$$\begin{aligned}&\left[\begin{pmatrix}0 & 1 & 1 & 0\\ -h & 0 & -3v^2\cos^2\theta-h & -h\\ h & 0 & 2 & 0\end{pmatrix}\partial_y\right.\\ &\qquad\left.+\frac{1}{6h}\begin{pmatrix}0 & -6h' & -3h' & 0\\ -3hh' & 18v^2\cos^2\theta h' & 3(3v^2\cos^2\theta+h)h' & 0\\ 2K^2yh & -12K^2v^2y\cos^2\theta & -2K^2y(3v^2\cos^2\theta-h) & 2K^2yh\end{pmatrix}\right]\begin{pmatrix}E_1\\ E_2\\ E_3\\ E_4\end{pmatrix}\\ &\qquad=\frac{h'}{4Kyh}e^{-iK_1\xi/z_H}\vartheta(y-y_*)\begin{pmatrix}-ivy\sec\theta\\ 3ivy\cos\theta(v^2+h)\\ K(v^2-h)\end{pmatrix}.\end{aligned} \tag{57}$$

To solve the 10 second order equations of motion for specified K, we must fix 20 integration constants.

- Think of 15 as being fixed at the boundary of AdS_5-Schwarzschild (that is, $y = 0$) and the remaining 5 at the horizon to suppress solutions describing gravitons coming *out* of the black hole.
- Of the 15 boundary conditions at $y = 0$, five come from imposing the first-order constraints. This is arbitrary: the constraints can be imposed anywhere.
- The 10 remaining boundary conditions at $y = 0$ come from requiring the metric of the boundary to remain Minkowski (at least in the absence of accidental creation of baby universes.)

In more detail (sorry):

Near the boundary, the leading behavior of H_{mn} is

$$H_{mn} = Q^{\rm tot}_{mn} y^4 + R_{mn} \,, \tag{58}$$

where R_{mn} is a deformation of the Minkowski metric which we set to 0 (that's 10 integration constants). The K-th co-moving Fourier component of the stress tensor can be read off from $Q^{\rm tot}_{mn}$:

$$\langle T_{mn} \rangle = \frac{\pi^2}{8} N^2 T^4 \, {\rm diag}\{3,1,1,1\} + \int \frac{d^3K}{(2\pi)^3} \langle T^K_{mn} \rangle e^{i\left[K_1(x^1 - vt) + K_2 x^2 + K_3 x^3\right]/z_H} \tag{59}$$

$$\langle T^K_{mn} \rangle = \frac{\pi^3 T^4 \sqrt{g^2_{YM} N}}{\sqrt{1-v^2}} Q^{\rm tot}_{mn} \,. \tag{60}$$

Imposing the first order constraints at small y gives five relations on $Q^{\rm tot}_{mn}$ which correspond to conservation and tracelessness of T_{mn} (almost—see the discussion following (66)!) Using in addition the vanishing of B_1, B_2, and C (obvious from the absence of source terms in (48) and (51)), one may express

$$Q^{\rm tot}_{mn} = a_{mn} Q^{\rm tot}_A + d_{mn} Q^{\rm tot}_D + e_{mn} Q^{\rm tot}_E + p_{mn} \tag{61}$$

in terms of just three numerically determined quantities: $Q^{\rm tot}_A$, $Q^{\rm tot}_D$, and $Q^{\rm tot}_E$, defined through the asymptotic behaviors

$$A = Q^{\rm tot}_A y^4 + \ldots \qquad D_1 = Q^{\rm tot}_D y^4 + \ldots \qquad E_1 = Q^{\rm tot}_E y^4 + \ldots \tag{62}$$

for small y. (To work out the mass of a finite string as indicated in exercise 9, you need to know that $E_i = Q^{\rm tot}_{E_i} y^4$ for $i = 1$ through 4, and $Q^{\rm tot}_E \equiv Q^{\rm tot}_{E_1}$.) The other quantities in (61) are

$$(a_{mn}) = \frac{v^2 \sin^2\theta}{2} \begin{pmatrix} 0 & 0 & 0 & \\ 0 & -2\sin^2\theta & \sin 2\theta & 0 \\ 0 & \sin 2\theta & -2\cos^2\theta & 0 \\ 0 & 0 & 0 & 2 \end{pmatrix} \tag{63}$$

$$(d_{mn}) = \frac{v}{2} \begin{pmatrix} 0 & 4\sin^2\theta & -2\sin 2\theta & 0 \\ 4\sin^2\theta & -2v\sin^2 2\theta & v\sin 4\theta & 0 \\ -2\sin 2\theta & v\sin 4\theta & 2v\sin^2 2\theta & 0 \\ 0 & 0 & 0 & 0 \end{pmatrix} \tag{64}$$

$$(e_{mn}) = \frac{1}{4}\begin{pmatrix} -4 & 4v\cos^2\theta & 2v\sin 2\theta & 0 \\ 4v\cos^2\theta & 4e_{11} & (1-3v^2\cos^2\theta)\sin 2\theta & 0 \\ 2v\sin 2\theta & (1-3v^2\cos^2\theta)\sin 2\theta & 4e_{22} & 0 \\ 0 & 0 & 0 & -2+2v^2\cos^2\theta \end{pmatrix} \tag{65}$$

$$e_{11} = \frac{1}{2}\left[-1+(1+v^2)\cos^2\theta - 3v^2\cos^4\theta\right]$$

$$e_{22} = \frac{1}{2}\cos^2\theta(-1-2v^2+3v^2\cos^2\theta)$$

$$(p_{mn}) = \frac{iv\cos\theta}{4K}\begin{pmatrix} 0 & 2v & 2v\tan\theta & 0 \\ 2v & -3+v^2+(1-3v^2)\cos^2\theta & \left[-2+(1-3v^2)\cos^2\theta\right]\tan\theta & 0 \\ 2v\tan\theta & \left[-2+(1-3v^2)\cos^2\theta\right]\tan\theta & 2-2v^2-(1-3v^2)\cos^2\theta & 0 \\ 0 & 0 & 0 & 1+v^2 \end{pmatrix} \tag{66}$$

All the terms in (61) are conserved except the last. The non-conservation of this last term precisely characterizes the total energy delivered to the thermal medium by the quark, which is acted upon by some external force so that it does not slow down: see the discussion following (45) of [23].

Detailed asymptotic forms near the horizon can also be found in [23], but it would add little to the current presentation to include them here. The boundary conditions at $y = 1$ suppressing outfalling solutions are standard for classical black hole horizons.

1. The barest summary of this technical discussion is that $Q_E^{\rm tot}$ is proportional to the K-th co-moving Fourier coefficient $\langle T_{00}^K \rangle$ of the energy density.
2. When $y_* = 0$ there is one more subtlety, namely a subtraction from $\langle T_{00}^K \rangle$ of the Coulombic near-field of the quark, which has infinite energy.
3. The subtracted quantity is the Q_E^K appearing in figure 19.

4. $Q_E^{\rm tot}$ is computed by solving a boundary value problem for ODE's in y from $y = 0$ (the boundary of AdS_5-Schwarzschild) to $y = 1$ (the horizon). Our implementation uses Mathematica's `NDSolve`.
5. Computing $Q_E^{\rm tot}$ for a single value of v and $\vec{K}$ takes about 15 seconds on a modern PC. A reasonably thorough scan of values takes several hundred CPU-hours.

It is possible to solve the E equations (56) in the limit of small K, where the sonic boom behavior of hydrodynamics should be reproduced. And it is:

$$Q_E^{\rm tot} = \frac{3iv(1+v^2)\cos\theta}{2K} \frac{1}{(1-3v^2\cos^2\theta)\left(1-\frac{ivK\cos\theta}{1+v^2}\right) - ivK\cos\theta} + O(K)\,. \tag{67}$$

See figure 19a.

For $K \sim 1$, where numerics is the only available method, broad directional peaking can be seen either from individual curves in figure 19c,d, or more comprehensively in figure 20.

Intriguingly, the results for light quarks (say with $y_* = 0.63$) are qualitatively similar to the results for heavy quarks with the near-field subtraction mentioned in point 2

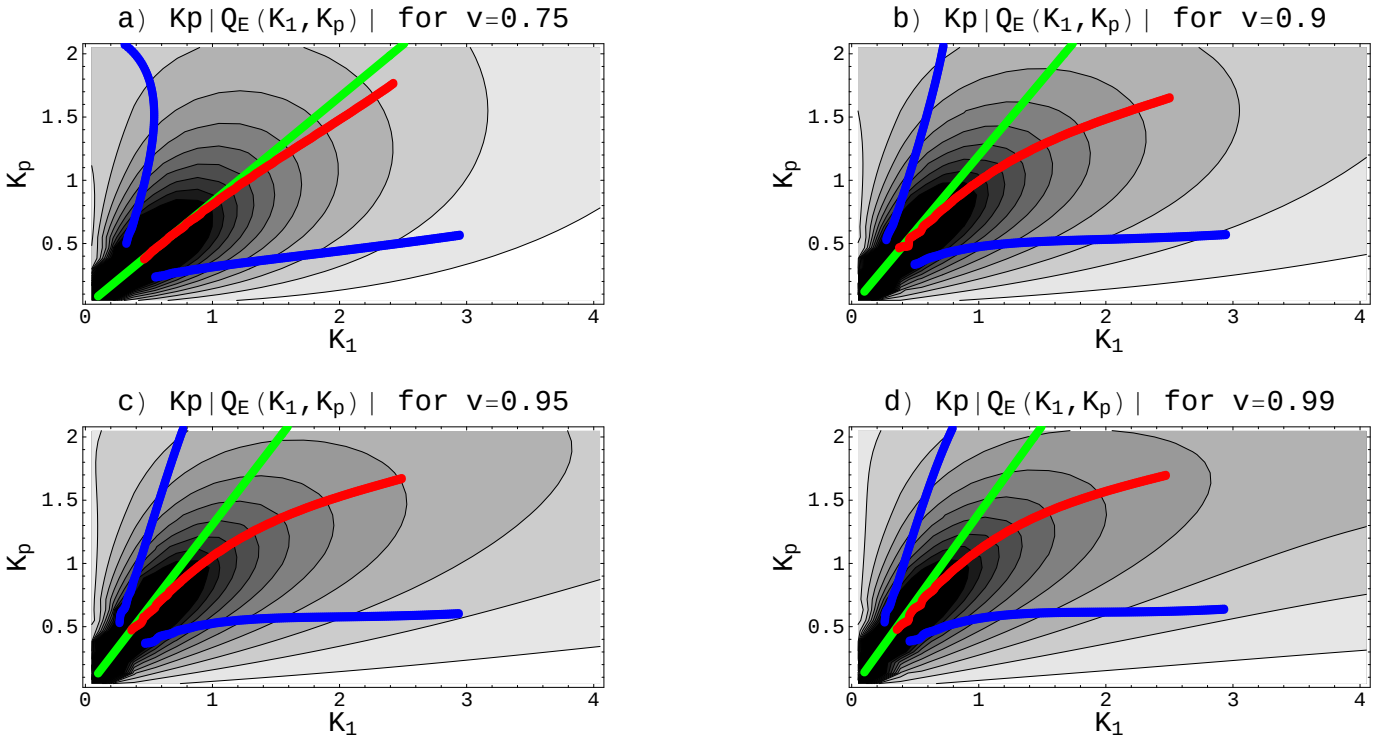

Figure 20: *Contour plots of $K_\perp|Q_E^K|$ for various values of v. Q_E^K is proportional to the K-th Fourier component of the energy density after a near-field subtraction. The phase space factor $K_\perp$ arises in Fourier transforming back to position space. The green line shows the Mach angle. The red curve shows where $K_\perp|Q_E^K|$ is maximized for fixed $K = \sqrt{K_1^2 + K_\perp^2}$. The blue curves show where $K_\perp|Q_E^K|$ takes on half its maximum value for fixed K. From [23].*

above.

- This is not wholly unexpected: the "light quarks" in question are trailing strings with a UV truncation.
- It's good news that light quark results agree qualitatively with the subtracted results for heavy quarks: the match between figures 18 and 19 is already reasonable.
- What bothers us is that the end of the string is travelling super-luminally along the flavor brane when $y_* > y_v = \sqrt[4]{1-v^2}$.
  - The worldsheet has signature -+, as it ought.
  - The issue is that the flavor brane boundary of the worldsheet is spacelike rather than timelike.
  - Heavy quarks don't have this problem because $y_* < y_v$.
  - The location $y = y_v$ is a sort of horizon for the induced metric on the comoving string worldsheet.

5. Conclusions

- A simple type IIB string configuration helps elucidate the physics of jet quenching at RHIC.
- Broadly directional peaks agree qualitatively with observed splitting of the away-side jet.
- The string theory setup involves significant idealizations of the experimental setup, notably replacing QCD by $\mathcal{N} = 4$ super-Yang-Mills.
- Nevertheless, we hope that further improvements may lead to more precise comparisons of string theory predictions with data.

6. Future directions

What's next for string theorists interested in RHIC physics—or for RHIC phenomenologists interested in string theory? We're not sure, but here are four things that seem particularly bothersome about the setup we have discussed so far:

1. The QGP at RHIC has finite extent, and it is rapidly expanding and cooling. That's in contrast with any calculation done in the static AdS_5-Schwarzschild background. Some recent works seek to improve this situation [35, 36].
2. The equation of state changes appreciably as the QGP turns into hadronic matter. This matters a lot in a hydrodynamic treatment: for instance, it significantly increases the Mach angle for sonic booms. See for example [29].
3. Type IIB strings cannot break, whereas the QCD string can break by popping a light $q\bar{q}$ pair into existence. Flavor branes help with this problem, but their 10-dimensional realization is not simple.
4. The precise relationship between Fourier coefficients of energy density (or other components of $\langle T_{mn} \rangle$) and the energy of measured hadrons is poorly understood, at least by us.

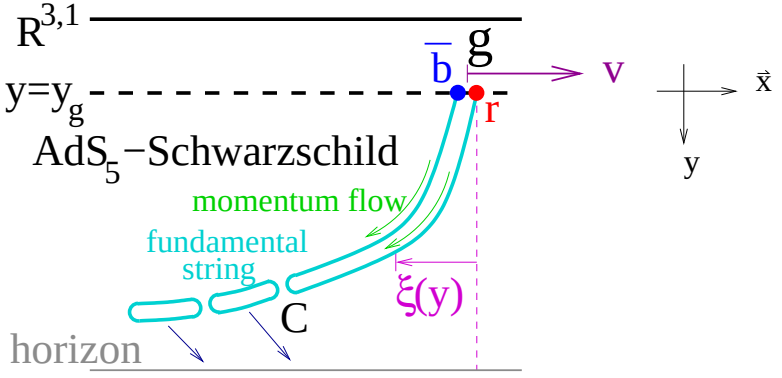

Figure 21: *Proposed description of a high-momentum gluon with color quantum numbers $R\overline{B}$. The string and anti-string are drawn as separate for illustration purposes only. Annihilation of the string-anti-string pair becomes appreciable at at point C roughly a string time from the ends of the string. The string fragments fall into the horizon, approximately following spacelike geodesics.*

6.1. String-anti-string annihilation

Point 3 above might be related to another conundrum for string theorists: *How should we represent a hard gluon traveling through the QGP?* This is interesting because hard partons (unless they are tagged as heavy quarks) will be gluons roughly as often as they are light quarks. We propose the following admittedly ad hoc picture: see figure 21.

- Represent the gluon as a coincident string-anti-string pair terminating on a test

brane at some $y = y_g$ and trailing toward the horizon.

- The adjoint charge of the gluon has to do with the Chan-Paton factors at the ends of the string.
- The string and anti-string will tend to annihilate each other.
- Annihilation takes a time t_C which is parametrically of order $\sqrt{\alpha'}$.
- The energy from the string-anti-string pair goes preferentially into highly excited closed strings which then follow ballistic trajectories into the horizon.
- Annihilation becomes important for those portions of the string which are a proper time greater than t_C from the endpoints of the string.
- Energy and momentum flows down the string to the point where it decays, and then are carried off by the decay products.

The real-time annihilation of a coincident string-anti-string pair is hard to understand in any quantitative detail.

- We are not in a weak coupling corner of type IIB moduli space: $g_s = g_{YM}^2/4\pi = \alpha_s$, and α_s in RHIC collisions is variously estimated to lie between 0.3 and 1.
- If g_s were *large*, we could S-dualize and try to adapt the discussion of S-branes in [37] to the current setup.
- In the limit of zero coupling (that is, $g_s \to \infty$ before S-dualizing) S-branes

decay into open strings at the Hagedorn temperature. This is one reason we believe the decay should be into highly excited string states.

- If g_s were *small*, then the string-anti-string configuration would have a small probability per unit length to split, resulting again in highly excited string states as the preferential decay products.
- A similar picture may describe the drag force on quarkonium systems. We are aware of work on related topics by another group [38].

So what should we calculate?

- The locus of points at a proper time $\sqrt{\alpha'}$ from the boundary of the string can shown to be specified by $y = y_C$, where

$$\int_{y_g}^{y_C} \frac{dy}{y} \sqrt{\frac{1-v^2}{v^2-h}} = \frac{\sqrt{\alpha'}}{L}, \tag{68}$$

  provided $y_g > y_v$.
- An educated guess for $\tau_{\mu\nu}$ of the string could be made based on the picture summarized above and in figure 21.
- Given $\tau_{\mu\nu}$ obeying the symmetries of the trailing string (i.e. co-moving with the gluon and with rotational symmetry around the axis of the gluon's motion), graviton perturbation calculations can be carried along the lines of section 4.4.

References

[1] B. Muller and J. L. Nagle, "Results from the Relativistic Heavy Ion Collider," nucl-th/0602029.

[2] **BRAHMS** Collaboration, I. Arsene *et. al.*, "Quark gluon plasma and color glass condensate at RHIC? The perspective from the BRAHMS experiment," *Nucl. Phys.* **A757** (2005) 1–27, nucl-ex/0410020.

[3] **PHENIX** Collaboration, K. Adcox *et. al.*, "Formation of dense partonic matter in relativistic nucleus nucleus collisions at RHIC: Experimental evaluation by the PHENIX collaboration," *Nucl. Phys.* **A757** (2005) 184–283, nucl-ex/0410003.

[4] B. B. Back *et. al.*, "The PHOBOS perspective on discoveries at RHIC," *Nucl. Phys.* **A757** (2005) 28–101, nucl-ex/0410022.

[5] **STAR** Collaboration, J. Adams *et. al.*, "Experimental and theoretical challenges in the search for the quark gluon plasma: The STAR collaboration's critical assessment of the evidence from RHIC collisions," *Nucl. Phys.* **A757** (2005) 102–183, nucl-ex/0501009.

[6] The full MPEG can be found at http://www.bnl.gov/RHIC/images/movies/Au-Au_200GeV.mpeg, where it is attributed to the UrQMD group at Frankfurt, see http://www.physik.uni-frankfurt.de/~urqmd/.

[7] M. Kaneta and N. Xu, "Centrality dependence of chemical freeze-out in Au + Au collisions at RHIC," nucl-th/0405068.

[8] **BRAHMS** Collaboration, I. G. Bearden *et. al.*, "Nuclear stopping in Au + Au collisions at s(NN)**(1/2) = 200-GeV," *Phys. Rev. Lett.* **93** (2004) 102301, nucl-ex/0312023.

[9] F. Karsch, "Lattice QCD at high temperature and density," *Lect. Notes Phys.* **583** (2002) 209–249, hep-lat/0106019.

[10] F. Wegner *J. Math. Phys.* **12** (1971) 2259.

[11] W. Zajc, private communication.

[12] M. D. Baker, "The latest Results from PHOBOS: Systematics of Charged Particle Production through $\sqrt{s_{NN}} = 200\,\mathrm{GeV}$," 2001. PowerPoint talk, available at http://www.phobos.bnl.gov/Presentations/paris01/.

[13] **PHENIX** Collaboration, S. S. Adler *et. al.*, "Centrality dependence of direct photon production in s(NN)**(1/2) = 200-GeV Au + Au collisions," *Phys. Rev. Lett.* **94** (2005) 232301, nucl-ex/0503003.

[14] S. S. Gubser, I. R. Klebanov, and A. W. Peet, "Entropy and Temperature of Black 3-Branes," *Phys. Rev.* **D54** (1996) 3915–3919, hep-th/9602135.

[15] G. Policastro, D. T. Son, and A. O. Starinets, "The shear viscosity of strongly coupled N = 4 supersymmetric Yang-Mills plasma," *Phys. Rev. Lett.* **87** (2001) 081601, hep-th/0104066.

[16] P. Kovtun, D. T. Son, and A. O. Starinets, "Viscosity in strongly interacting quantum field theories from black hole physics," *Phys. Rev. Lett.* **94** (2005) 111601, hep-th/0405231.

[17] S. R. Das, G. W. Gibbons, and S. D. Mathur, "Universality of low energy absorption cross sections for black holes," *Phys. Rev. Lett.* **78** (1997) 417–419, hep-th/9609052.

[18] A. Buchel, "On universality of stress-energy tensor correlation functions in supergravity," *Phys. Lett.* **B609** (2005) 392–401, hep-th/0408095.

[19] http://www.bnl.gov/bnlweb/pubaf/pr/PR_display.asp?prID=05-38.

[20] S. S. Gubser, "Dilaton-driven confinement," hep-th/9902155.

[21] C. P. Herzog, A. Karch, P. Kovtun, C. Kozcaz, and L. G. Yaffe, "Energy loss of a heavy quark moving through N = 4 supersymmetric Yang-Mills plasma," hep-th/0605158.

[22] S. S. Gubser, "Drag force in AdS/CFT," hep-th/0605182.

[23] J. J. Friess, S. S. Gubser, G. Michalogiorgakis, and S. S. Pufu, "The stress tensor of a quark moving through N = 4 thermal plasma," hep-th/0607022.

[24] **PHENIX** Collaboration, S. S. Adler *et. al.*, "Modifications to di-jet hadron pair correlations in Au + Au collisions at s(NN)**(1/2) = 200-GeV," nucl-ex/0507004.

[25] K. Peeters, J. Sonnenschein, and M. Zamaklar, "Holographic melting and related properties of mesons in a quark gluon plasma," hep-th/0606195.

[26] H. Liu, K. Rajagopal, and U. A. Wiedemann, "An AdS/CFT calculation of screening in a hot wind," hep-ph/0607062.

[27] M. Chernicoff, J. A. Garcia, and A. Guijosa, "The energy of a moving quark-antiquark pair in an N = 4 SYM plasma," hep-th/0607089.

[28] Talk by B. Jacak, "Plasma physics of the quark gluon plasma", Boulder, May 2006. Available at http://www4.rcf.bnl.gov/∼steinber/boulder2006/.

[29] J. Casalderrey-Solana, E. V. Shuryak, and D. Teaney, "Conical flow induced by quenched QCD jets," *J. Phys. Conf. Ser.* **27** (2005) 22–31, hep-ph/0411315.

[30] A. Majumder and X.-N. Wang, "LPM interference and Cherenkov-like gluon bremsstrahlung in dense matter," *Phys. Rev.* **C73** (2006) 051901, nucl-th/0507062.

[31] V. Koch, A. Majumder, and X.-N. Wang, "Cherenkov radiation from jets in heavy-ion collisions," *Phys. Rev. Lett.* **96** (2006) 172302, nucl-th/0507063.

[32] A. K. Chaudhuri and U. Heinz, "Effect of jet quenching on the hydrodynamical evolution of QGP," nucl-th/0503028.

[33] J. Ruppert and B. Muller, "Waking the colored plasma," *Phys. Lett.* **B618** (2005) 123–130, hep-ph/0503158.

[34] J. J. Friess, S. S. Gubser, and G. Michalogiorgakis, "Dissipation from a heavy quark moving through N = 4 super- Yang-Mills plasma," hep-th/0605292.

[35] R. A. Janik and R. Peschanski, "Asymptotic perfect fluid dynamics as a consequence of AdS/CFT," *Phys. Rev.* **D73** (2006) 045013, hep-th/0512162.

[36] S. Nakamura and S.-J. Sin, "A holographic dual of hydrodynamics," hep-th/0607123.

[37] A. Strominger, "Open string creation by S-branes," hep-th/0209090.

[38] M. Edalati, private communication.

[39] **STAR** Collaboration, C. Adler *et. al.*, "Coherent rho0 production in ultra-peripheral heavy ion collisions," *Phys. Rev. Lett.* **89** (2002) 272302, nucl-ex/0206004.

[40] J. B. Kogut, "An introduction to lattice gauge theory and spin systems," *Rev. Mod. Phys.* **51** (1979) 659.

7. Answers to selected exercises

Exercise 1, page 6

With $R = 7\,\mathrm{fm}$ one gets $6.1\,\mathrm{barn}$ from the geometric overlap formula. This means 2.5×10^{10} collisions. We don't know what the triggering efficiencies are, or how many of these events wind up on tape. [39]

Exercise 2, page 7

In the table below most of the interesting numbers are shown. The percentage in the decay modes indicates the ratio Γ_i/Γ. Only the major decay modes are shown and the decay modes for the negatively charged pions are the charge conjugates of the positive ones.

particle	mass/MeV	mean life/s	charge	isospin	quark content	decay modes
$\pi^{\pm}$	139.57	2.6×10^{-8}	± 1	1	$u\bar{d}, \bar{u}d$	$\mu^+\nu_\mu$ 99.9%
π^0	134.97	8.4×10^{-17}	0	1	$(u\bar{u} - d\bar{d})/\sqrt{2}$	$\gamma\gamma$ 98.80%, $e^+e^-\gamma$ 1.2%
K_S^0	497	0.89×10^{-10}	0	1/2	$(d\bar{s} + \bar{d}s)/\sqrt{2}$	$\pi^+\pi^-$ 69.20%, $\pi^0\pi^0$ 30.69%
K_L^0	497	5.11×10^{-8}	0	1/2	$(d\bar{s} - \bar{d}s)/\sqrt{2}$	$\pi^{\pm}e^{\mp}\nu_e$ 40.53%, $\pi^{\pm}\mu^{\mp}\nu_\mu$ 27.02%
ϕ	1019.46	16×10^{-23}	0	0	$s\bar{s}$	K^+K^- 49.2%, $K_S^0K_L^0$ 34.0%
p	938.27	stable?	+1	1/2	uud	
n	939.57	885.7	0	1/2	udd	$pe^-\bar{\nu}_e$ 100%
Λ	1115.68	2.63×10^{-10}	0	0	uds	$p\pi^-$ 63.9%, $n\pi^0$ 35.8%
Σ^+	1189.37	0.802×10^{-10}	+1	1	uus	$p\pi^0$ 51.6%, $n\pi^+$ 48.3%
Σ^0	1192.64	7.4×10^{-20}	0	1	uds	$\Lambda\gamma$ 100%
Σ^-	1197.45	1.48×10^{-10}	-1	1	dds	$n\pi^-$ 99.85%
Ξ^0	1314.83	2.90×10^{-10}	0	1/2	uss	$\Lambda\pi^0$ 99.52%
Ξ^-	1321.3	1.64×10^{-10}	-1	1/2	dss	$\Lambda\pi^-$ 99.89%
Ω^-	1672.5	0.82×10^{-10}	-1	0	sss	ΛK^- 67.8%, $\Xi^0\pi^-$ 23.6%
D^+	1869.3	1040×10^{-15}	± 1	1/2	$c\bar{d}$, $\bar{c}d$	$\bar{K}_0e^+\nu_e$ 8.6% $\bar{K}_0\mu^+\nu_\mu$ 9.5%
D^0	1864.5	410×10^{-15}	0	1/2	$c\bar{u}$	K anything 53%
J/ψ	3096.91	1.5×10^{-20}	0	0	$c\bar{c}$	hadrons 87.7% e^+e^- 5.94%, $\mu^+\mu^-$ 5.93%

Exercise 3, page 7

PHENIX's angular acceptance is $70.3^\circ < \theta < 109.3^\circ$, and the forward muon detectors cover $10.4^\circ < \theta < 27.7^\circ$, relative to the beamline.

Exercise 4, page 7

Since $\cos\theta = p_z/|p| \approx p_z/E$ when $p_z \gg m$, we find $\tanh\eta = \cos\theta \approx p_z/E = \tanh y$.

To show the effect of Lorentz boosts on rapidity, first note that $\tanh y = p_z/E = \gamma\beta_z m/(\gamma m) = \beta_z$. If one boosts by $\hat{\beta}_z$, then the new β is

$$\beta_z' = \frac{\beta_z + \hat{\beta}_z}{1 + \beta_z\hat{\beta}_z}$$

This can be verified by using Lorentz transformation formulae for energy-momentum and computing p_z'/E'. Then recall that

$$\tanh(y + \hat{y}) = \frac{\tanh y + \tanh\hat{y}}{1 + \tanh y \tanh\hat{y}}$$

So rapidity is indeed shifted by a constant through the relation $\tanh\hat{y} = \hat{\beta}_z$.

Exercise 5, page 12

A gauge transformation is to flip the signs associated to all four links meeting at a given point. The solution to the Wilson loop problem can be found in section V.D of [40], and proceeds as follows.

The quantity of interest is

$$\begin{aligned}\left\langle \prod_{l\in C} s_l \right\rangle &= \frac{\sum_{\text{configurations}} \exp\left(\beta \sum_{\text{plaquettes}} s_{p_1}s_{p_2}s_{p_3}s_{p_4}\right) \prod_{l\in C} s_l}{\sum_{\text{configurations}} \exp\left(\beta \sum_{\text{plaquettes}} s_{p_1}s_{p_2}s_{p_3}s_{p_4}\right)} \\ &= \frac{\sum_{\text{configs}} \prod_{\text{plaq's}} (1 + s_{p_1}s_{p_2}s_{p_3}s_{p_4}\tanh\beta) \prod_{l\in C} s_l}{\sum_{\text{configs}} \prod_{\text{plaq's}} (1 + s_{p_1}s_{p_2}s_{p_3}s_{p_4}\tanh\beta)}\end{aligned} \tag{69}$$

Now, consider high T, i.e., small β. Then this quantity can be expanded in powers of β. Since $\sum_{\text{configs}} s = 0$ and $\sum_{\text{configs}} s^2 = 2$, a given term in the sum in the numerator will vanish if there is an "unpaired" factor of s_i at a given link site i along the curve C. It can be shown therefore that the first non-zero contribution to the numerator comes from the term where one factor of $s_{p_1} s_{p_2} s_{p_3} s_{p_4} \tanh\beta$ is included for each plaquette inside C. This can easily be checked for the case of C surrounding just two plaquettes. Consequently we find

$$\left\langle \prod_{l\in C} s_l \right\rangle \propto (\tanh\beta)^A + \cdots, \qquad \text{for} \beta \ll 1$$

Higher order corrections will maintain this area-law behavior.

At low temperatures, the dominant configuration has all the links with the same sign, and the Wilson loop expectation value is just 1. Consider thermal perturbations around this configuration. If n spins are flipped, the action increases by $2n\beta$. If one of these spins happens to be along the curve C, then the Wilson loop value is -1. If the lattice has N links, and the length of the Wilson loop is L, then there are $N^n/n!$ distinct configurations with n flipped signs, which gets modified to $(N-L)^n/n!$ in the numerator to account for the Wilson loop. Consequently we find:

$$\left\langle \prod_{l\in C} s_l \right\rangle = \frac{\sum_{n=0}^{\infty} \frac{1}{n!}(N-L)^n \exp(-2n\beta)}{\sum_{n=0}^{\infty} \frac{1}{n!} N^n \exp(-2n\beta)} = e^{-2L\exp(-2\beta)}$$

Exercise 6, page 20

The equation of motion for $\hat{\phi}$ is clearly $\Box\hat{\phi} = 0$, so $\hat{\phi} = \hat{\phi}_0$ is a solution. Furthermore, the dilaton contribution to Einstein's equations will be proportional to $(\partial\hat{\phi})^2$, which is zero. So, we can set the dilaton to a constant and forget about it.

The form field's contribution to the action is:

$$S \sim \int d^{10}x\sqrt{\hat{G}}|\hat{F}_5^2| = \int \hat{F}_5 \wedge \star \hat{F}_5$$

So, the equation of motion is simply $d \star \hat{F}_5 = 0$, just as two of Maxwell's equations can be written as $d \star dA = 0$, where A is the gauge potential. We can express the self-duality condition, $F_5 = \star F_5$, by writing $F_5 = f_5 + \star f_5$, where now f_5 is an arbitrary 5-form. We want a solution with a 5-sphere, so by the symmetries of the problem, f_5 must have its indices all on the sphere or all on AdS_5. We'll take f_5 to be along $AdS - Schwarzschild$. Furthermore, recall that f_5 actually comes from a 4-form potential $\hat{A}_4$. Then the equation of motion reads

$$d \star \hat{F}_5 = d(f_5 + \star f_5) = d \star f_5 = 0$$

By Gauss's law on the 5-sphere, we have

$$\int_{S^5} \star f_5 = N$$

where N is an integer that essentially counts the D-brane charge. This determines f_5 completely once the metric is known.

Einstein's equations, found from varying the action, give the solution for the metric, which can be written as the following Ansatz:

$$ds^2 = e^{2A(z)}\left(-e^{2B(z)}dt^2 + d\vec{x}^2 + e^{-2B(z)}dz^2\right) + e^{2C(z)}L^2 d\Omega_5^2$$

The only trick is that the F_5^2 term in Einstein's equations should be set to zero, after varying the action, as part of the self-duality constraint.

Again by the symmetries, there are four independent Einstein's equations – three second order equations coming from the $t-t$, $x-x$, and $\theta-\theta$ components, and a first order gauge constraint from the $z-z$ component. Three of these equations determine the functions A, B, and C, and the fourth should determine the relationship between the number of D-branes N and the AdS radius L.

Exercise 7, page 21

The N^2 in (12) should really have been N^2-1 because the gauge group is $SU(N)$. N^2 was used because it is what supergravity gives. With this adjustment, one obtains $s = \frac{16\pi^2}{3}T^3$ for $\mathcal{N}=4$. The QCD case with three flavors is laid out carefully in (2) of [3] and gives $s = \frac{19\pi^2}{12}T^3$, which is smaller by a factor of about 0.30.

Exercise 8, page 25

Viscosity is a measure of the internal friction and can be defined by $T_{zx} = \eta\frac{\partial v}{\partial z}$. We only have to calculate the left hand side. The particle number per unit surface per unit time is nv_{th} and so the momentum per unit surface per unit time is $nv_{th}mv$. T_{zx} is the difference between the fluxes in an imaginary box of length $v_{th}\tau_{mfp}$. Each flux is $nv_{th}m(v_0 \pm v_{th}\tau_{mfp}\frac{\partial v}{\partial z})$ so $T_{zx} \sim nv_{th}^2 m\tau_{mfp}\frac{\partial v}{\partial z}$ and $\eta \sim \epsilon\tau_{mfp}$.

The fact that this is the correct relativistic extrapolation can be checked by the fact that $\epsilon \to \gamma\epsilon$ and $\tau \to \tau/gamma$. Normally $\epsilon \to \gamma^2\epsilon$, since both mass and number density pick up a factor of γ. However, the thermal velocity is quite large, so there is already a large γ factor in the energy density from the mass factor, so for boosts much less than the thermal velocity, this γ factor does not get significantly increased, and hence only number density picks up a factor of γ.

ptExercise 9, page 33

A simple route to (24) is explained in section 3.1 of [21]. The point of the second part is to understand the translation of total energy in AdS_5-Schwarzschild to $\int d^3x \, \langle T_{00} \rangle$ in the gauge theory. The relevant equation of motion is actually fairly simple:

$$\mathcal{L} E_3 = -\frac{y}{h} \theta(y - y_*) \qquad \mathcal{L} \equiv \partial_y^2 + \left(-\frac{3}{y} + \frac{h'}{2h} \right) \partial_y \,. \tag{70}$$

The solutions to the homogenous equation $\mathcal{L} g = 0$ are $g = 1$ and $g = \sqrt{h}$. Because these solutions are so simple, the method of Green's functions seems an obvious approach. Recall the general result that $\mathcal{L}_y G(y; y_p) = \delta(y - y_p)$ is solved by

$$G(y; y_p) = \frac{1}{W(y_p)} \begin{cases} g_+(y_p) g_-(y) & \text{for } y < y_p \\ g_-(y_p) g_+(y) & \text{for } y > y_p \end{cases} \qquad W(y) \equiv g_+'(y) g_-(y) - g_-'(y) g_+(y) \tag{71}$$

where g_+ and g_- are any two linearly independent solutions to the homogenous equation. The vanishing of E_3 at the boundary of AdS_5-Schwarzschild forces us to take $g_-(y) = 1 - \sqrt{h}$. The horizon boundary conditions are not as obvious. Let us follow our noses and set $g_+(y) = \sqrt{h}$, which is the smaller of the two solutions. We mostly want to compute the behavior of E_3 at small y, so it is interesting to note that for small y,

$$G(y; y_p) \approx \frac{h(y_p)}{h'(y_p)} y^4 \,. \tag{72}$$

From

$$E_3 = -\int_0^1 dy_p \, G(y; y_p) \frac{y_p}{h(y_p)} \theta(y_p - y_*) \approx -\frac{y^4}{4} \int_{y_*}^1 \frac{dy_p}{y_p^2} \tag{73}$$

we may read off

$$Q^{\rm tot}_{E_3} = \frac{1}{4}\left(\frac{1}{y_*} - 1\right) = -\frac{1}{2}Q^{\rm tot}_{E_1} \equiv -\frac{1}{2}Q^{\rm tot}_{E}\,. \tag{74}$$

Strangely, if we had computed $Q^{\rm tot}_{E_1}$ directly with similar methods from the equation of motion for E_1, with horizon boundary conditions chosen again to correspond to the smaller of the two homogeneous solutions, we would not arrive at (74). It would be interesting to understand properly the boundary conditions on E_1 at the horizon.

In any case, we are now in a position to finish the calculation by noting that the total energy is

$$\begin{aligned}\int d^3x\,\langle T_{00}\rangle &= \frac{1}{\pi^3 T^3}\langle T_{00}^{K=0}\rangle = -T\sqrt{g^2_{YM}N}\,Q^{\rm tot}_E = T\frac{\sqrt{g^2_{YM}N}}{2}\left(\frac{1}{y_*}-1\right)\\ &= \frac{\sqrt{g^2_{YM}N}}{2\pi}\left(\frac{1}{z_*}-\frac{1}{z_H}\right) = \frac{L^2}{2\pi\alpha'}\left(\frac{1}{z_*}-\frac{1}{z_H}\right).\end{aligned} \tag{75}$$

The unexpected factor of $1/\pi^3T^3$ in the first equality is because of the definition of $\vec{K} = \vec{k}/\pi T$.

Exercise 10, page 39

The answer is found by simple integration. Approximating $6.3/5 \approx 5/4$, and $\hbar c = 198 MeV\,fm$, we find

$$n_{\rm stop} = 2\pi\sqrt{2}\frac{250}{1188}(\sqrt{5}-1)\sqrt{\frac{\lambda}{10}}\left(\frac{1500MeV}{m}\right) \approx 2.31\sqrt{\frac{\lambda}{10}}\left(\frac{1500MeV}{m}\right)$$